machines

MDPI

Article

Design, Calibration, and Troubleshooting of a Modular Low-Cost 3D Printer Based on Open-Source Technologies

Mauricio Arturo Moreno-Gerena [1], Luis Manuel Navas-Gracia [2,*] and Juan Gonzalo Ardila-Marín [2,3]

[1] SIMEX S.A.S, Carrera. 48 #48 Sur 181, Envigado 055422, Colombia; mauricio.moreno@simex.com.co
[2] TADRUS Research Group, Department of Agricultural and Forestry Engineering, Universidad de Valladolid, UVa Campus of Palencia, 34004 Palencia, Spain; juan.ardila@usco.edu.co
[3] Program of Agricultural Engineering, Faculty of Engineering, Universidad Surcolombiana, USCO Sede Central, Pastrana Borrero Avenue, Carrera 1, Neiva 410001, Colombia
* Correspondence: luismanuel.navas@uva.es

Abstract

This paper presents the design, construction, and calibration of a modular low-cost 3D printer based on open-source technologies, developed as part of an academic research project. The printer utilises fused filament fabrication (FFF) and is built using locally available materials and components, including a T-slot aluminium frame, NEMA 23 stepper motors, and an Arduino Mega 2560 with RAMPS 1.4 control board. The system integrates Marlin firmware and CURA slicing software, enabling autonomous operation via an LCD panel and encoder interface. A detailed methodology is provided for mechanical assembly, electronic integration, firmware configuration, and calibration procedures. Special attention is given to the challenges encountered during the initial testing phase, including filament feeding issues, thermal inconsistencies, and mechanical misalignments. Solutions such as replacing inadequate components (e.g., fibreglass bushings with PTFE), adjusting spring tension, and refining firmware parameters are discussed. The results demonstrate successful printing of complex geometries after iterative calibration, validating the printer's performance and replicability. This work contributes to the democratisation of additive manufacturing by offering a replicable, open-source solution for educational and prototyping purposes. The findings are relevant to machine design, automation, and robotics communities seeking practical insights into low-cost fabrication systems.

Keywords: motion control; Human–Machine Interface (HMI); embedded firmware; parametric design; automated calibration; power electronics; modular architecture

Academic Editors: Raul D. S. G. Campilho and Nicola Ivan Giannoccaro

Received: 21 January 2026
Revised: 14 February 2026
Accepted: 21 February 2026
Published: 25 February 2026

1. Introduction

The potential of layer-based manufacturing to optimise design workflows, reduce development time and costs, and foster the emergence of enterprises based on automated technologies was already recognised by Ardila Marín in 2007 [1]. Since then, the proliferation of additive manufacturing through open-source platforms has significantly contributed to democratising access to digital fabrication and prototyping tools, particularly in low-resource environments. Nevertheless, technical and economic barriers continue to hinder its widespread adoption. Several studies have identified the high cost of commercial 3D printers as a central issue, with prices exceeding USD 500,000 for metal-based

systems [2] and reaching up to USD 200,000 for soft-material printers [3], figures that effectively exclude laboratories, small enterprises, and rural communities. Although the RepRap movement has promoted low-cost solutions, critical challenges remain in the construction, calibration, and operation of these systems. For instance, Laplume et al. (2016) report failure rates of up to 20% in open-source printers [4], while Khan et al. (2025) demonstrate that technical errors can compromise geometric accuracy by as much as 3.34% [5]. Furthermore, studies by Keller et al. (2025) [6] and Jadayel (2024) [7] show that insufficient calibration can lead to systematic errors of up to ±150 μm, adversely affecting print quality in complex geometries. However, work such as that of Ahmad et al. (2020) [8] reinforced that additive manufacturing enables the accurate reproduction of complex forms, such as anatomical structures, while reducing fabrication time and eliminating intermediate processing steps, underscoring its growing relevance in technical and educational applications. In this context, there is a clear need to document replicable technical procedures that enable the construction and optimisation of low-cost modular 3D printers, enhancing their functionality and educational utility in non-specialised environments.

Since the earliest developments of open-source 3D printers, the RepRap movement has inspired numerous research initiatives aimed at democratising additive manufacturing. Anzalone et al. (2013) proposed a low-cost metal printer based on MIG welding, reducing the cost of commercial equipment to under USD 2000 [2]. Although their technical approach validated the feasibility of metal deposition, it did not address calibration procedures or educational replicability. In parallel, Wittbrodt et al. (2013) conducted a life-cycle economic analysis of a RepRap printer, demonstrating annual savings ranging from USD 300 to USD 2000 [9], yet without considering the technical challenges that may hinder the realisation of such benefits. Schuh (2024) documented the construction and calibration of an FFF printer using recycled materials, offering a pedagogical perspective that underscores the educational value of projects built around Marlin firmware and Arduino platforms [10].

In subsequent years, Gwamuri et al. (2016) emphasised the potential of open-source 3D printers in rural communities, proposing energy solutions such as solar power and plastic recycling [11]. While their focus was primarily socio-economic, they did not explore the technical design or operational calibration aspects. Laplume et al. (2016) and Petersen and Pearce (2017) delved into business models [4] and return-on-investment analyses [12], respectively, but left unexamined the technical factors that underpin printer functionality.

Geometric accuracy has been another key area of investigation. Minetola et al. (2018) assessed improvements in Prusa i3 printers using self-replicated components, achieving performance levels comparable to professional-grade equipment according to ISO IT classification [13]. Rendón-Medina et al. (2018) validated the clinical use of low-cost FDM printers, reporting a dimensional error of 1.96% [14]. However, both studies focused on geometric outcomes without addressing user experience or operational failures, such as filament jams or bed levelling issues. Rosli et al. (2018), Sood and Pradhan (2019), and Nath et al. (2020) explored metal-material printers [15], parameter optimisation for PLA [16], and FFF process optimisation under uncertainty using physics-informed models [17], respectively. These studies reinforced the need for precise calibration to enhance process reliability across conventional and non-conventional materials yet did not detail the practical challenges of assembly and configuration. Kechagias et al. (2022) provided a comprehensive review of the parameters influencing surface quality and dimensional accuracy in FFF, highlighting the complexity of their interactions and the necessity for systematic control methodologies [18]. Similarly, Erokhin et al. (2023) classified common defects in FFF printing and proposed mitigation strategies [19].

More recently, Weiss et al. (2025) developed a multimaterial printer for biofabrication, validating its precision (±5 μm) and cell viability (>95%) [3], although they did not elaborate on the mechanical calibration processes. Jadayel (2024) and Keller et al. (2025) proposed computational and optical methods to improve geometric accuracy, achieving enhancements of up to 88.5% [7] and error reductions by a factor of 1.7 [6], respectively. While their approaches are metrological and computational in nature, they do not address replicability in educational contexts or the use of accessible components.

Other studies have addressed dynamic control and automation. Weiss (2013) proposed a closed-loop control system to enhance trajectory precision [20]; Ctibor et al. (2018) improved stepper motor control in Arduino-based printers [21]; and Salazar-Serrano et al. (2018) automated optical mounts using printed components [22]. These works share a common interest in accessible and precise systems, yet do not apply their solutions directly to the geometric calibration of FFF printers. Praja et al. (2020) [23], Khona et al. (2022) [24], Schuh (2024) [10] and Khan et al. (2024) [5] documented construction and testing processes using Marlin firmware, but without in-depth technical analysis of thermal performance or evaluation of critical parameters.

Finally, studies such as those by Campana et al. (2021) and Dupont et al. (2021) have explored sustainability [25] and collaborative manufacturing [26], respectively, highlighting the environmental impact of self-replication and the potential of the "Do-It-Together" model. Although they share an interest in technological decentralisation, they do not incorporate energy systems or alternative materials such as agricultural residues. Tolentino et al. (2024) and Gibb and Pearce (2025) further reinforce the relevance of open-source hardware in education and research [27,28], yet fail to document replicable technical processes or applications in rural contexts.

In this context, this article documents the design, construction, calibration and troubleshooting of a modular low-cost 3D printer based on open-source technologies, developed within an academic project on technological development. The central hypothesis posits that it is possible to build a functional and replicable additive manufacturing system using exclusively accessible components and open-source platforms, without compromising print quality in complex geometries. To validate this hypothesis, the methodological procedures followed in the project are described, including the mechanical and electronic design of the system, firmware and control software integration, calibration of critical printing parameters, and the identification and resolution of recurrent faults during initial testing. The results obtained allow for an evaluation of the system's performance and its potential as an educational and prototyping tool in resource-limited environments.

This work offers a comprehensive engineering development study. The primary contribution resides in the formalisation of practical engineering procedures and replicable workflows, aligning with fundamental benchmarks that prioritise technical documentation. Our approach is inspired by the seminal works of Anzalone et al. (2013) [2] and Hallgren and Wiberg (2015) [29], who validated that providing exhaustive documentation for "derivative" open-source designs is essential for technological democratisation and user-driven innovation. Similar to the case studies by Kayfi et al. (2015) [30] and Veliu et al. (2024) [31], this paper serves as an educational reference and a practical implementation guide for integrating OSH components into functional R&D environments. We further integrate the perspective of Dunn et al. (2023) [32] regarding the viability of self-produced, complex hardware, demonstrating how community-driven modifications strengthen design stability. Furthermore, following the empirical findings of Omer et al. (2024) [33], we address the critical need for context-specific design modifications to ensure global replicability in resource-constrained settings, where "minor adjustments" are often the key to functional success. By aligning with these practical precedents, our research

provides the necessary technical infrastructure to transform a modular design into a real-world tool.

2. Materials and Methods

The 3D printer developed in this project was conceived using a modular approach, which enabled its design to be divided into mechanical, electronic, and control subsystems. This strategy not only facilitated the construction and assembly process, but also enhances its maintenance, scalability, and replicability in educational or low-budget contexts [34,35].

The mechanical design was developed using Autodesk Inventor 2014® software (Autodesk Inc., San Rafael, CA, USA), allowing for the 3D modelling of each component, the generation of technical drawings, and the anticipation of interferences or adjustments prior to fabrication. Figure 1 provides an annotated overview of the mechanical architecture of the system. Figure 1a highlights the structural layout of the T-slot aluminium frame, including the main junction points and alignment features that ensure geometric stability during assembly. Figure 1b shows the complete CAD assembly with labelled subsystems—X, Y, and Z carriages, extruder module, build platform, and electronics tray—to support clear identification of functional components. These annotations were added to enhance readability and to facilitate replication of the mechanical configuration by external users. This CAD-based methodology is widely employed in rapid prototyping and digital manufacturing projects [36–38].

The printer features a usable print volume of 300 × 300 × 200 mm, a dimension selected for its versatility in producing medium-sized functional parts. This working area falls within the typical range of desktop FFF printers aimed at educational and prototyping applications [5,39,40]. The assembled machine has overall external dimensions of approximately 502 × 686 × 571 mm (width × depth × height).

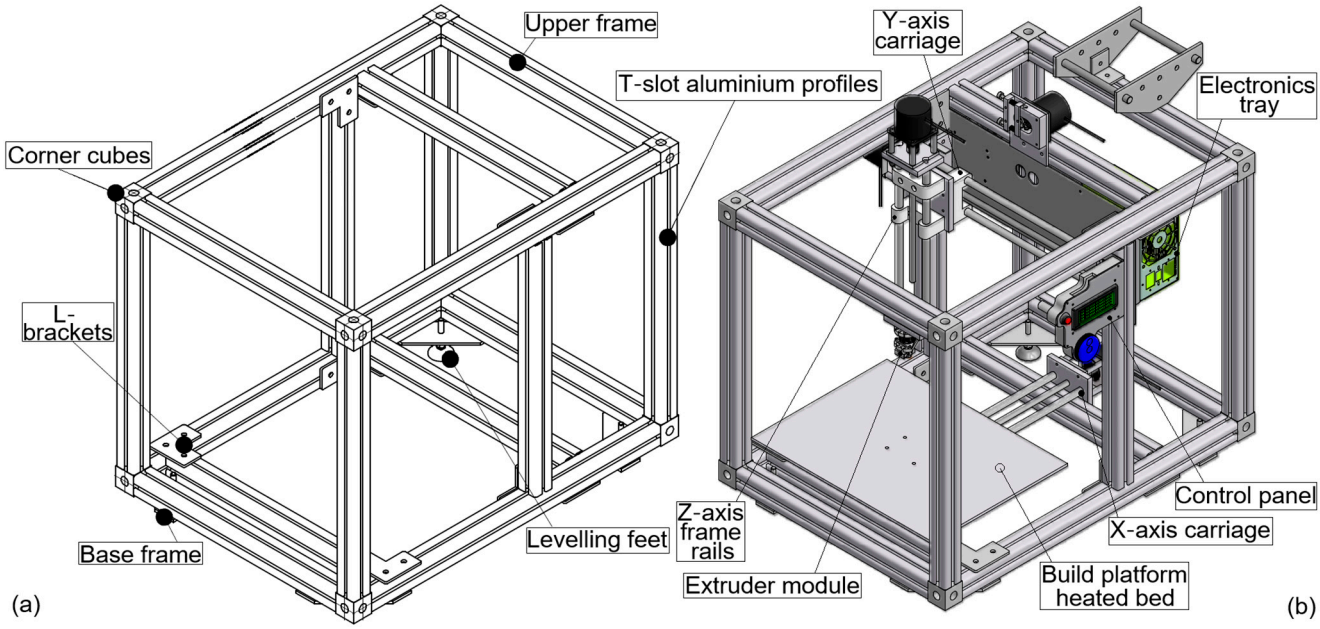

Figure 1. Modular architecture of the 3D printer: (**a**) annotated T-slot aluminium frame highlighting structural joints and alignment elements; (**b**) complete CAD assembly with labelled subsystems, including axis carriages, extruder module, electronics tray, and build platform.

From its initial conception, the system was designed to be low-cost, employing materials and components readily available in the regional market. The total material cost of

the complete prototype was approximately USD 350–450, depending on the local availability of components such as T-slot aluminium profiles for the frame, NEMA 23 stepper motors (standard 23HS-series model supplied by Wantai Motor Co., Ltd., Beijing, China) and the ATX power supply (Shenzhen XinLong Electronics Co., Ltd., Shenzhen, China), and an electronics setup based on the Arduino Mega 2560 (Arduino S.r.l., Turin, Italy), paired with the RAMPS 1.4 board (Geeetech, Shenzhen, China) and A4988 drivers (Pololu Corporation, Las Vegas, NV, USA). This hardware combination is widely adopted within the RepRap community and has proven to be both reliable and economical [10,21,41,42].

Regarding software, open-source tools commonly used in the 3D printing community were selected. The slicing software, Ultimaker Cura 14.07 (Ultimaker B.V., Utrecht, The Netherlands) was chosen for its user-friendly interface and compatibility across multiple platforms, while the Marlin firmware was configured to manage critical printing parameters such as steps per unit, travel limits, speeds, and sensor inputs [23,43–45].

For the fabrication of components, accessible processes such as laser cutting, conventional milling, and turning were employed. This choice was driven by the local availability of services and the need to keep costs low without compromising the system's functionality. The firmware folder, design files and supporting documentation used in this study are available in the public repository cited in the Data Availability Statement.

2.1. Mechanical Components

The mechanical system of the 3D printer was designed with a modular and functional approach, prioritising ease of assembly, maintenance, and replicability. Each subsystem was conceived to fulfil a specific role within the fused filament fabrication (FFF) process, ensuring precision, stability, and compatibility with low-cost components.

2.1.1. Frame

The main frame is constructed using T-slot aluminium profiles, which are widely used in automation and robotics applications due to their versatility and ease of assembly [41,46–48]. This type of profile allows for precise adjustments in component positioning and facilitates system expansion or modification.

The structure consists of a lower and upper frame, joined by perforated corner cubes and L-brackets, providing rigidity and stability to the assembly. Levelling feet are integrated into the base to ensure proper alignment of the print plane. This modular design enables the movement of the X, Y, and Z axis carriages with precision along linear guides. The designed structure is shown in Figures 1a and 2d.

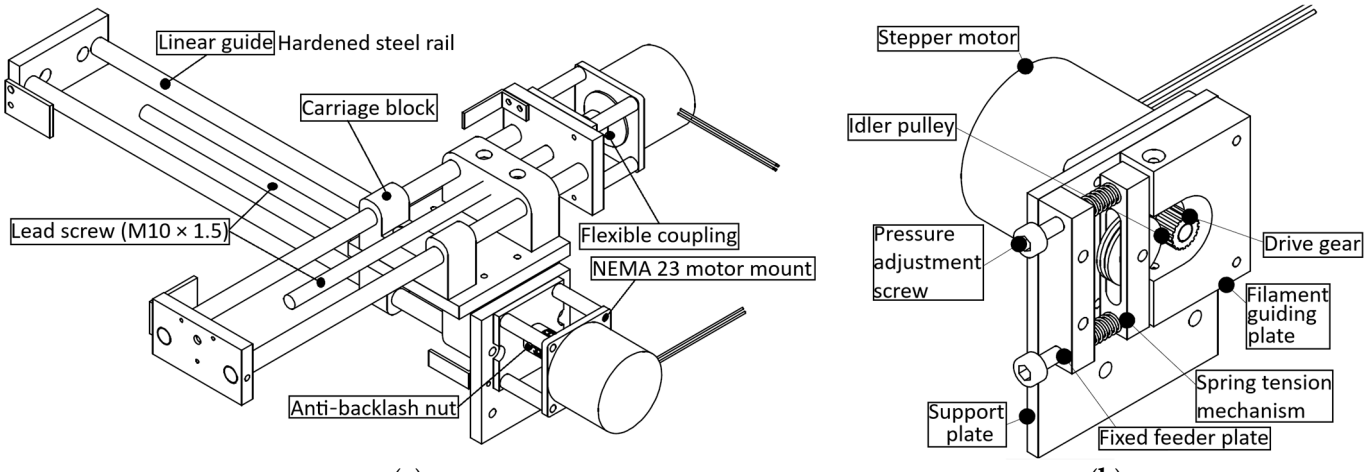

(**a**) (**b**)

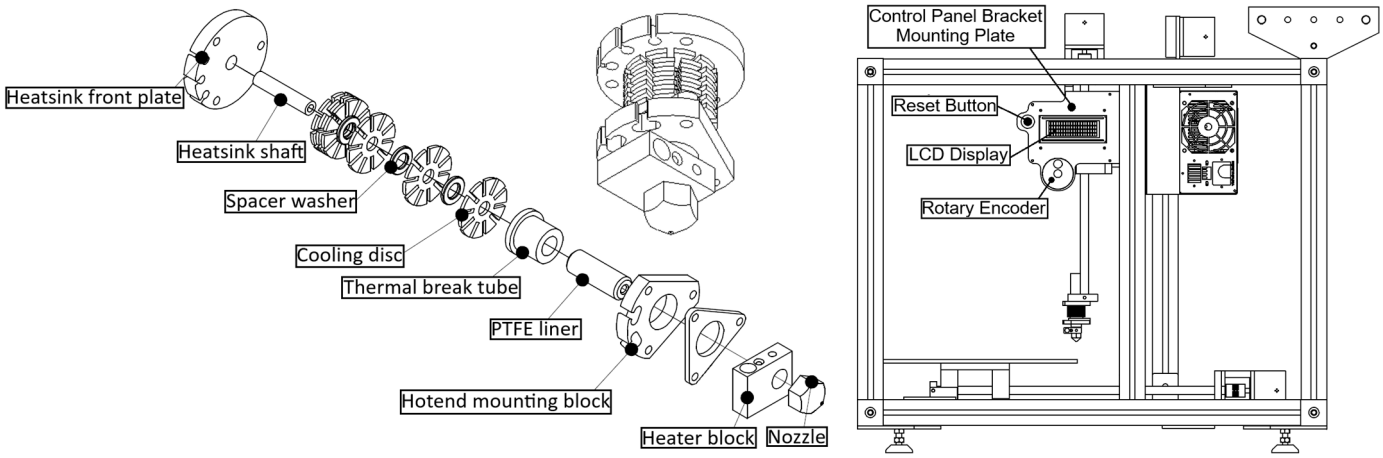

(**c**) (**d**)

Figure 2. Annotated mechanical subsystems of the 3D printer: (**a**) Y–Z axis carriages with labelled linear guides, lead screws, and couplings; (**b**) filament feeding mechanism showing drive gear, idler, and tension system; (**c**) extruder assembly with identified thermal components; (**d**) modular frame and control interface with marked modules.

2.1.2. X, Y, and Z Axis Carriages

The carriages are designed to move along hardened steel linear guides, driven by M10 × 1.5 threaded rods and NEMA 23 stepper motors (Wantai Motor Co., Ltd., Beijing, China). This configuration enables precise positioning across the three Cartesian axes, a critical feature in FFF systems [23,40,47,49]. Each carriage comprises side mounting plates, guiding blocks, and nuts coupled to the threaded rods. The design includes flexible couplings between the motors and rods to compensate for potential misalignments, thereby reducing mechanical wear and enhancing system durability. The CAD models of the Y and Z carriages are shown in Figure 2a with labelled linear guides, carriage blocks, lead screws, flexible couplings, and motor mounts, allowing readers to clearly identify the elements responsible for multi-axis motion and alignment.

2.1.3. Filament Feeding System

The filament feeding system consists of a stepper motor that drives the filament through a gear and pulley assembly with spring-loaded tension adjustment. This mechanism ensures consistent filament feeding to the extruder, minimising the risk of clogs or slippage. A CAD representation of the system is shown in Figure 2b, where the filament feeding mechanism includes annotations identifying the drive gear, idler pulley, tension adjustment system, filament guiding plate, support plate, feeder mounting plate, spacer washer. These labels clarify how filament is constrained, driven, and stabilised before entering the hotend.

2.1.4. Extruder

The extruder is based on the Budaschnozzle 1.3 model, with custom modifications to enhance its performance. It comprises a set of heat sinks, a heating block with a resistor and thermistor, and a 0.5 mm nozzle. The filament is guided through a PTFE tube, which acts as a thermal insulator and reduces internal friction. A schematic 3D model of the extruder is presented in Figure 2c with detailed labels indicating the heatsink front plate, cooling discs (heatsink fins), central mounting shaft, PTFE liner, thermal break tube, hotend mounting block, heater block, and nozzle. The design follows the open-source Budaschnozzle 1.3 specification, originally created by LulzBot/Aleph Objects, Inc. (Loveland, CO, USA), but the assembly used in this work was self-fabricated and modified.

2.1.5. Control Panel and Component Mounting

The control panel enables autonomous operation of the printer via an LCD screen, a rotary encoder, and a reset button. It is mounted on an adjustable stainless-steel plate. The electronic system (comprising the Arduino Mega 2560–Arduino S.r.l., Turin, Italy, RAMPS 1.4 board–Geeetech, Shenzhen, China, and A4988 drivers–Pololu Corporation, Las Vegas, NV, USA) is housed in a ventilated metal tray, ensuring adequate heat dissipation. A front view of the structure, including the control panel layout, is shown in Figure 2d with labels highlighting the LCD interface, rotary encoder, reset button, and mounting plate. Structural frame elements already described in Figure 1 are omitted here to maintain focus on user-interaction and control features relevant for standalone operation.

2.2. Electronic Components

The electronic system of the 3D printer was designed based on open-source hardware platforms, which allowed for cost reduction, simplified programming, and ensured compatibility with a wide range of control software. The architecture comprises a controller board, an expansion shield, stepper motor drivers, position sensors, and a human–machine interface system.

2.2.1. Controller Board: Arduino Mega 2560

The main board used is an Arduino Mega 2560, based on the ATmega2560 microcontroller (Microchip Technology Inc., Chandler, AZ, USA). Figure 3a illustrates the board, highlighting its primary communication ports and pin groups. This view emphasises the interfaces most relevant to the printer's control architecture, including USB communication, power input, analogue inputs and PWM-enabled digital outputs, which serve as the foundation for signal routing within the RAMPS 1.4 shield. This platform is widely adopted in 3D printing projects due to its processing capacity, number of input/output pins, and compatibility with firmware such as Marlin [38,50–52].

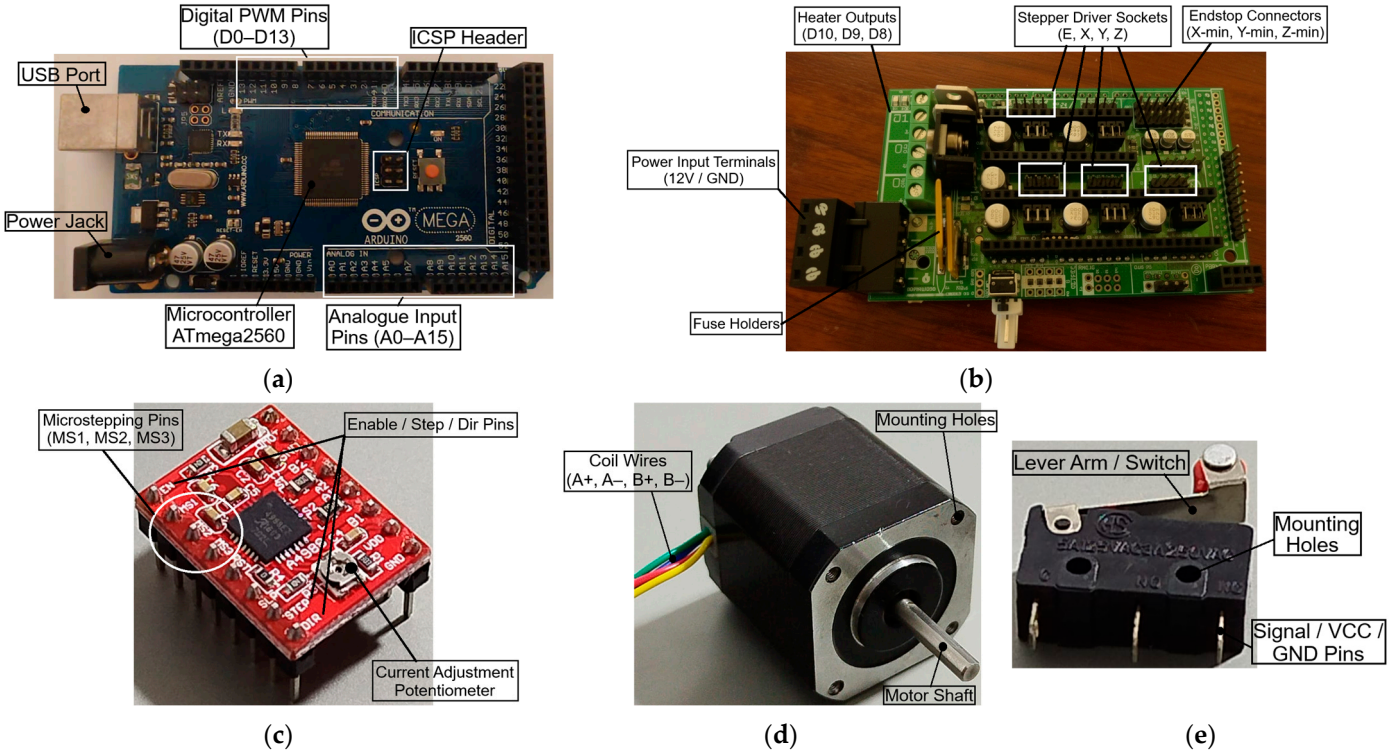

Figure 3. Annotated electronic components of the control system: (**a**) Arduino Mega 2560 with labelled USB port, power jack, microcontroller, ICSP header, analogue inputs, and digital PWM pins;

(**b**) RAMPS 1.4 shield showing power input terminals, stepper-driver sockets, heater outputs, fuse holders, and endstop connectors; (**c**) A4988 stepper driver with microstepping pins, current adjustment potentiometer, logic-signal pins, and heatsink; (**d**) NEMA 23 stepper motor with annotated shaft, coil wires, mounting holes, and specification label; (**e**) mechanical endstop switch with labelled signal pins, actuator lever, and mounting holes.

2.2.2. Expansion Shield: RAMPS 1.4

The Arduino board (Arduino S.r.l., Turin, Italy) is complemented by a RAMPS 1.4 shield (Geeetech, Shenzhen, China), which follows the open-source RepRap Arduino Mega Pololu Shield specification, and acts as an interface between the microcontroller and the power components. Figure 3b annotated to identify its principal connection terminals and driver sockets. This view clarifies the power distribution layout, heater outputs, fuse locations and endstop connectors, ensuring that readers can accurately replicate the wiring scheme and the integration of the motion-control subsystems. This shield enables the connection of motor drivers, temperature sensors, endstops, and other peripherals. Its modular design and widespread adoption within the RepRap community make it a standard choice for DIY (Do It Yourself) 3D printers [10,41,53–55].

2.2.3. Motor Drivers: A4988 Pololu

To control the stepper motors, A4988 drivers (Pololu Corporation, Las Vegas, NV, USA) were used. These drivers support microstepping up to 1/16 step, feature adjustable current control, and include overcurrent and overtemperature protection. As shown in Figure 3c with labelled functional elements, including microstepping configuration pins, the current-adjustment potentiometer and logic-signal terminals. This information is essential for correctly tuning torque, motion smoothness and thermal performance during axis and extruder operation. They are widely used in 3D printers due to their low cost and ease of integration [21,41,56,57].

2.2.4. Stepper Motors

To ensure precise and reliable movement of the printer's Cartesian axes, the required torque for the stepper motors was calculated, considering load conditions, friction, mechanical efficiency, and the characteristics of the leadscrew transmission system. The total required torque comprises two main components: load torque and acceleration torque. The expression used for the calculation is presented in Shigley et al. (2004) [58], is shown in Equation (1).

$$M = F\left(\frac{h}{2\pi\eta} + r_B\mu_B\right) \quad (1)$$

where M: Total required torque [N·cm]; F: Total axial force [N]; h: Leadscrew pitch [cm]; η: Transmission system efficiency; r_B: Mean bearing radius [cm]; and μ_B: Bearing friction coefficient. For the X-axis, with a load mass of approximately 1.5 kg, a leadscrew pitch of 1.5 mm, and typical friction coefficients for steel–bronze contact, the required torque was calculated to be approximately 2.70 N·cm. This value was obtained without considering gear reduction or preload, representing a conservative estimate. A NEMA 23 stepper motor was selected, with the following technical specifications: Step angle: 1.8°; Steps per revolution: 200; Rated current: 2.8 A; Holding torque: 0.9 N·m (90 N·cm); Inductance: 1.2 mH; Resistance: 0.8 Ω; Shaft diameter: 6.35 mm; and Weight: 0.6 kg. This motor was chosen with a generous safety margin, enabling not only efficient axis movement but also the potential integration of additional tools such as cutting heads or dual extruders in future prototype versions.

Moreover, these bipolar NEMA 23 motors (Wantai Motor Co., Ltd., Beijing, China) were selected for their torque and compatibility with A4988 drivers (Pololu Corporation,

Las Vegas, NV, USA). Figure 3d shows the external features of the stepper motor, indicating the shaft, mounting interface and coil-wire connections. These annotations support correct mechanical alignment and electrical phasing, which are critical for achieving stable and repeatable motion across the X, Y and Z axes. These motors allow for precise positioning control of the X, Y, and Z axes, as well as the filament feeding system [47,49,59,60]. Their operation is based on the switching of internal coils via control signals generated by the firmware.

2.2.5. Position Sensors: Endstops

Each axis is equipped with two endstop switches (generic KW11-type, sourced from Geeetech, Shenzhen, China) minimum and maximum, as shown in Figure 3e, which define the travel limits and enable the homing operation. The Figure presents the mechanical endstop, with labels identifying the actuator lever and the signal–VCC–GND pin arrangement. This view assists users in correctly orienting and wiring the homing sensors, thereby ensuring reliable axis referencing during system calibration. These mechanical sensors are connected to the RAMPS 1.4 board (Geeetech, Shenzhen, China) and are managed by the firmware to prevent collisions and ensure system repeatability.

2.3. Firmware and Control Software

The printer's control system is based on open-source tools widely adopted by the 3D printing community, ensuring flexibility, continuous updates, and compatibility with open hardware platforms.

2.3.1. Firmware: Marlin

The firmware selected for this project is Marlin (MarlinFirmware Project, GitHub Open-Source Community, USA), a robust and optimised solution for Arduino-based 3D printers [6,10,23,43]. Marlin enables the management of axis kinematics, extrusion, temperature control, and communication with slicing software. Its most notable features include: PID control for hotend and heated bed temperature regulation; Support for SD cards and LCD displays; Flexible configuration of steps per unit, travel limits, and speeds; and Algorithms for linear acceleration and curve compensation. Figure 4a illustrates the initial section of the Configuration.h file within the Arduino IDE, highlighting the firmware metadata, electronics board selection and baud-rate definition. These parameters form the foundation of the Marlin firmware configuration, and their correct setup is essential before adjusting motion parameters, endstop logic or travel limits in the subsequent sections of the file.

2.3.2. Slicing Software: CURA

In this study, Ultimaker Cura version 14.07 (released in 2014) was used to generate the G-code, converting 3D models into printer instructions. CURA is an open-source slicing software developed and maintained by Ultimaker B.V. (The Netherlands), widely adopted in the FFF 3D-printing community for its cross-platform compatibility and ease of configuration. CURA allows the configuration of critical parameters such as layer height, print speed, infill percentage and pattern, extruder and bed temperature, and support generation and auxiliary structures. Its intuitive interface and compatibility with multiple operating systems make it a standard tool for FFF printers [44,53]. Figure 4b shows the CURA Preferences window, highlighting the machine-dimension fields (build volume), extruder count, filament-density and cost parameters, and the serial-port and baud-rate communication settings. These configurations must remain consistent with the firmware settings to ensure correct printer communication and material handling. Figure 4c presents the JOG control window in CURA, showing the directional movement

controls for the X, Y and Z axes, as well as the manual plastic extrusion and retraction buttons. The Connect, Print and Pause controls and the printing statistics panel are also visible. These elements allow users to verify axis response, movement direction and extrusion behaviour during initial setup, and homing.

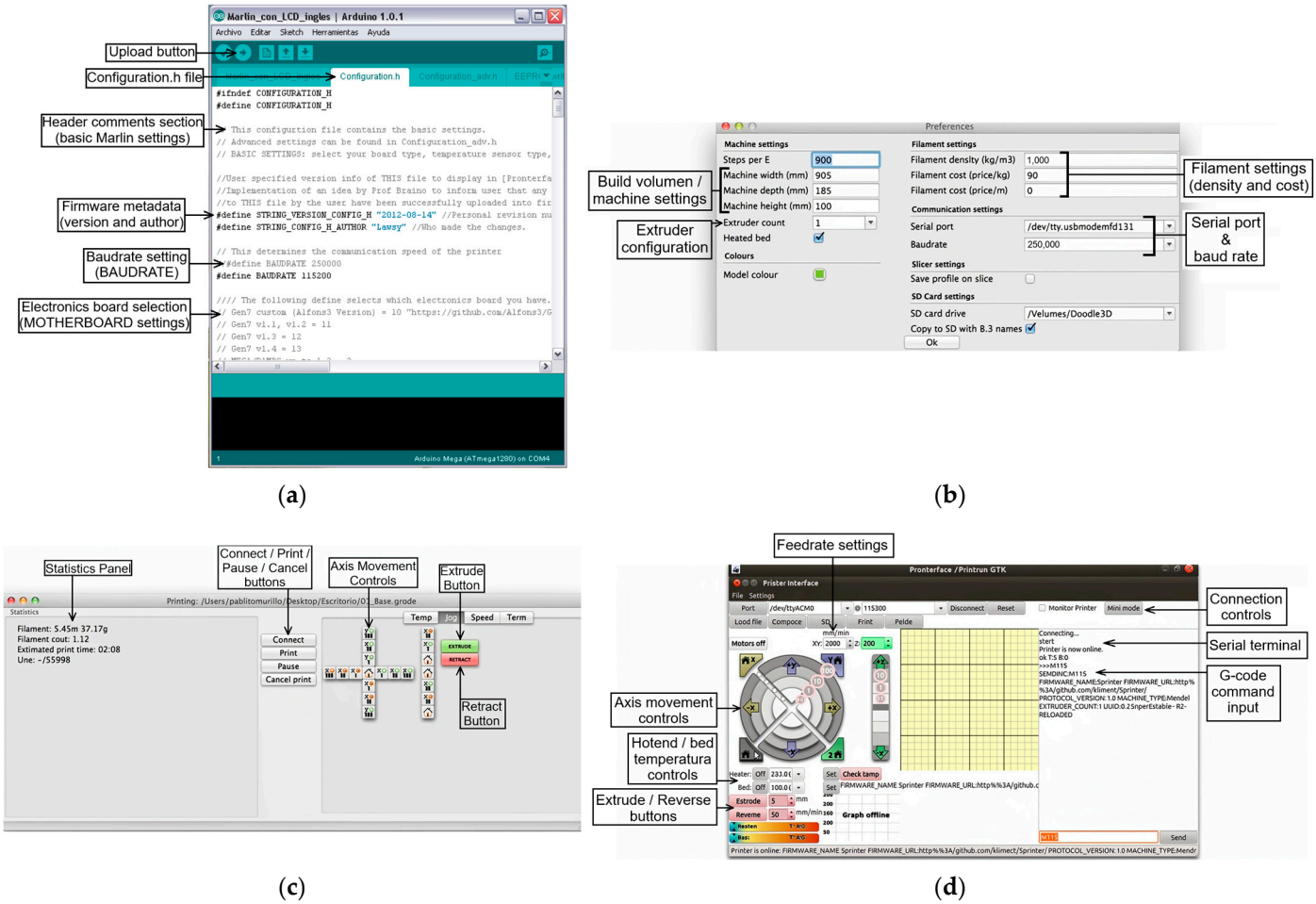

Figure 4. Annotated software interfaces supporting configuration and calibration: (**a**) Arduino IDE showing key firmware parameters (metadata, motherboard selection, baud rate); (**b**) Cura Preferences panel with build-volume fields, extruder count, filament settings, and communication parameters; (**c**) Cura JOG window with axis-movement controls and extrusion/retraction buttons; (**d**) Pronterface interface with jog controls, feed rate selection, temperature settings, manual extrusion panel, and G-code console.

2.3.3. Communication and Calibration

Communication between the firmware and software is established via USB connection using a serial protocol. The initial setup includes Serial port and baud rate configuration, Calibration of steps per unit for each axis, Adjustment of travel limits and maximum speeds, and Validation of endstop logic. These parameters are modified in the Configuration.h file of the Marlin firmware and verified through testing in the CURA environment and complementary tools such as Pronterface [61–63]. Figure 4d shows the Pronterface interface used during calibration and diagnostic procedures. The annotated elements include the axis-movement controls, feed rate settings, temperature controls for the hotend and heated bed, manual extrusion buttons, printer-connection controls, and the G-code terminal for real-time communication with the firmware. These features enable precise verification of motion behaviour, temperature response and extrusion performance. The

programmed extrusion length was then used to calibrate the feed rate and adjust the firmware steps-per-unit accordingly.

Table 1 summarises the main technical specifications of the developed 3D printer, including mechanical components, electronics, firmware configuration, and operational parameters. This consolidated view aims to support reproducibility and complements the detailed subsystem descriptions provided in Sections 2.1–2.3.

Table 1. Technical specifications of the developed modular 3D printer.

Overall dimensions	~502 × 686 × 571 mm (W × D × H)
Usable printing volume	300 × 300 × 200 mm
Frame	T-slot aluminium profiles (modular assembly)
Axes	Cartesian architecture: X, Y, Z
Linear guides	Hardened steel rods with carriage blocks (X, Y, Z)
Transmission	M10 × 1.5 threaded rods + flexible couplings
Motors	NEMA 23 stepper motors (1.8°, 90 N·cm holding torque, 2.8 A)
Extruder model	Modified Budaschnozzle 1.3
Hotend components	Heatsink, thermal break, PTFE liner, heater block, 0.5 mm nozzle
Feeding system	Drive gear + idler + spring-loaded tensioner
Electronics	Arduino Mega 2560 + RAMPS 1.4 + A4988 drivers
Power supply	ATX 12 V, 750 W
Sensors	Mechanical endstops (NC), thermistor
Firmware	Marlin (steps/mm, travel limits, PID tuning configured)
Slicing software	CURA (layer height, speed, infill, temperature configured)
Communication	USB serial protocol @ 115200 baud
Bed surface	5 mm glass plate
Validated temperatures	70 °C warm-up/190 °C PLA printing
Measured motion accuracy	±0.2 mm (axes), ±0.1 mm (homing)
Motion parameters	50 mm/s print speed, 3,000 mm/s^2 acceleration, jerk setting of 20 mm/s
Post-calibration dimensional error	≤0.5%
Cost	USD 350–450

2.4. Assembly Procedure

The assembly of the 3D printer followed a logical and modular sequence, aimed at ensuring the correct integration of mechanical and electronic subsystems. The process began with the construction of the main frame using T-slot aluminium profiles, which facilitated the alignment and positioning of components. The Y and Z axis carriages were then installed, followed by the X-axis and the base plate. Once the mechanical structure was complete, the filament feeding system and extruder were mounted, along with the material spool holder. Finally, the electronic components (including the control board, drivers, and user interface) were integrated into the system.

The modular nature of the design significantly simplified the assembly process, allowing for independent installation and testing of each subsystem. This approach not only reduced assembly time but also enhanced accessibility for future maintenance and potential upgrades.

2.5. Adjustments and Calibration

Calibration is a critical stage to ensure dimensional accuracy and surface quality of the printed parts. This process involves mechanical, electrical, and software adjustments to synchronise axis movement, material extrusion, and thermal control.

2.5.1. Axis and Endstop Adjustment

The movement direction of the X, Y, and Z axes was verified using manual commands in the control software (see Figure 4c). In cases of reversed motion, the corresponding variables were modified in the Marlin firmware. Subsequently, the endstops were adjusted to ensure that each axis correctly identifies its home position.

2.5.2. Print Bed Levelling

The print bed was levelled using a 5 mm glass plate placed on the base platform. The extruder height was adjusted to maintain a uniform gap of 0.1 mm at all four corners, ensuring a consistent first layer and proper adhesion [18,64].

2.5.3. Extruder and Filament Feed Calibration

The Pronterface software (Printrun package, Kliment Yanev and contributors, open-source community, USA) was used to calibrate the amount of extruded filament (see Figure 4d) [65–67]. The procedure involved commanding the extrusion of a specific length (e.g., 100 mm) and measuring the actual filament displacement. In case of discrepancies, the steps per unit were adjusted in the firmware using a simple proportional calculation. Real measurements were taken using a calliper. The procedure consisted of sending a movement command from the interface software (CURA or Pronterface), measuring the actual physical displacement, and adjusting the steps per unit accordingly. The formula applied is shown in Equation (2).

$$New\ value = \frac{Actual\ value \times Expected\ displacement}{Actual\ displacement} \quad (2)$$

This calibration method follows the standard RepRap procedure, which relies on proportional correction of the extrusion steps-per-unit based on measured filament displacement. This approach is widely adopted in open-source FFF printers because the extrusion mechanism behaves approximately linearly over the range of operational loads and temperatures.

Additionally, mechanical adjustments were made to the feeding system to improve filament tension. Figure 5a illustrates the mechanical intervention performed on the filament-feeding support block, showing the installed tension springs, compression screws and lock nuts, along with the original spring that was replaced due to insufficient stiffness. This annotated view clarifies the specific components involved in the pressure-regulation mechanism, thereby improving the transparency and reproducibility of the corrective action taken to eliminate filament slippage. The calibration procedure is detailed in Section 3.4.3, where the results of the adjustments are presented.

2.5.4. Temperature and Print Parameter Adjustment

The thermal system was tested by setting the hotend temperature to 70 °C and then to 190 °C for PLA printing. Thermistor readings were compared with external measurements using a thermocouple to validate thermal stability. Subsequently, parameters such as layer height, print speed, and infill percentage were configured in the CURA software (Ultimaker B.V., Utrecht, The Netherlands). To verify dimensional calibration, a test piece was printed. Figure 5b presents the calibration test piece used for dimensional verification following the mechanical and firmware adjustments. The annotated nominal dimensions

(25 × 4 mm) and the highlighted measurement areas support the evaluation of dimensional accuracy and layer uniformity, ensuring that the validation procedure can be reliably reproduced by other users.

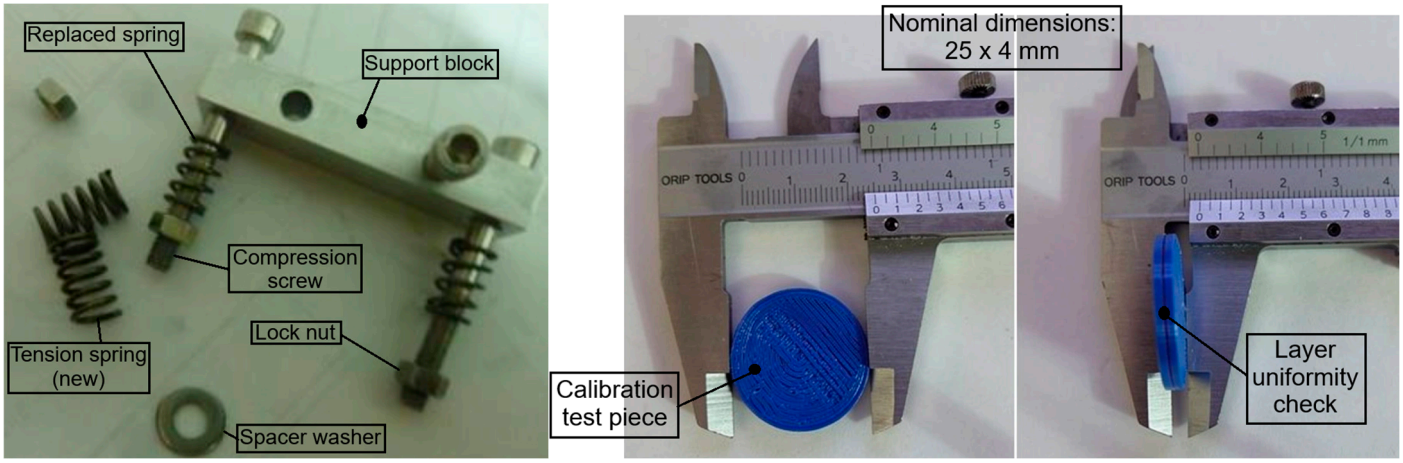

Figure 5. Mechanical adjustment of the feeding system and dimensional-verification test piece: (**a**) annotated feeding-system support block showing the installed tension springs, compression screws, lock nuts and the original spring replaced due to insufficient stiffness; (**b**) calibration test piece with nominal dimensions (25 × 4 mm) and indicated measurement areas for dimensional and layer-uniformity verification.

2.6. Validation Approach

The validation strategy adopted in this work focuses on internal functional verification of the developed prototype rather than comparative benchmarking against commercial or open-source printers. This decision aligns with the scope of engineering development studies, in which the objective is to assess the operability, calibration consistency, and troubleshooting processes of the newly developed system.

2.7. Use of Generative AI

During the preparation of this manuscript, the authors used Microsoft Copilot (GPT-4 architecture, Microsoft Corporation, Redmond, WA, USA) to assist in the drafting and refinement of specific sections. Additionally, some images were refined using AI-powered inpainting tools from OpenArt (OpenArt AI, San Francisco, CA, USA) to enhance resolution and legibility. The authors have reviewed and edited the output and take full responsibility for the content of this publication.

3. Results

3.1. Assembly and Connection of Electronic Components

The control system of the 3D printer is based on a modular open-hardware architecture, integrating an Arduino Mega 2560 board, a RAMPS 1.4 expansion shield, Pololu A4988 stepper motor drivers, endstop sensors, a thermistor, a heating resistor, an LCD control panel with rotary encoder, and a 12 V ATX power supply. The electrical design was structured to facilitate assembly, maintenance, and future upgrades. Figure 6 shows the complete electrical wiring diagram of the 3D printer, detailing the connections between the Printed Base Board, the stepper motors for the X, Y and Z axes, the extruder heater, the thermocouple input, the heated-bed circuit and the main 11A/5A power rails. This annotated schematic clarifies the organisation of the power and signal lines and

provides a reproducible reference for the assembly and integration of the electronic subsystem.

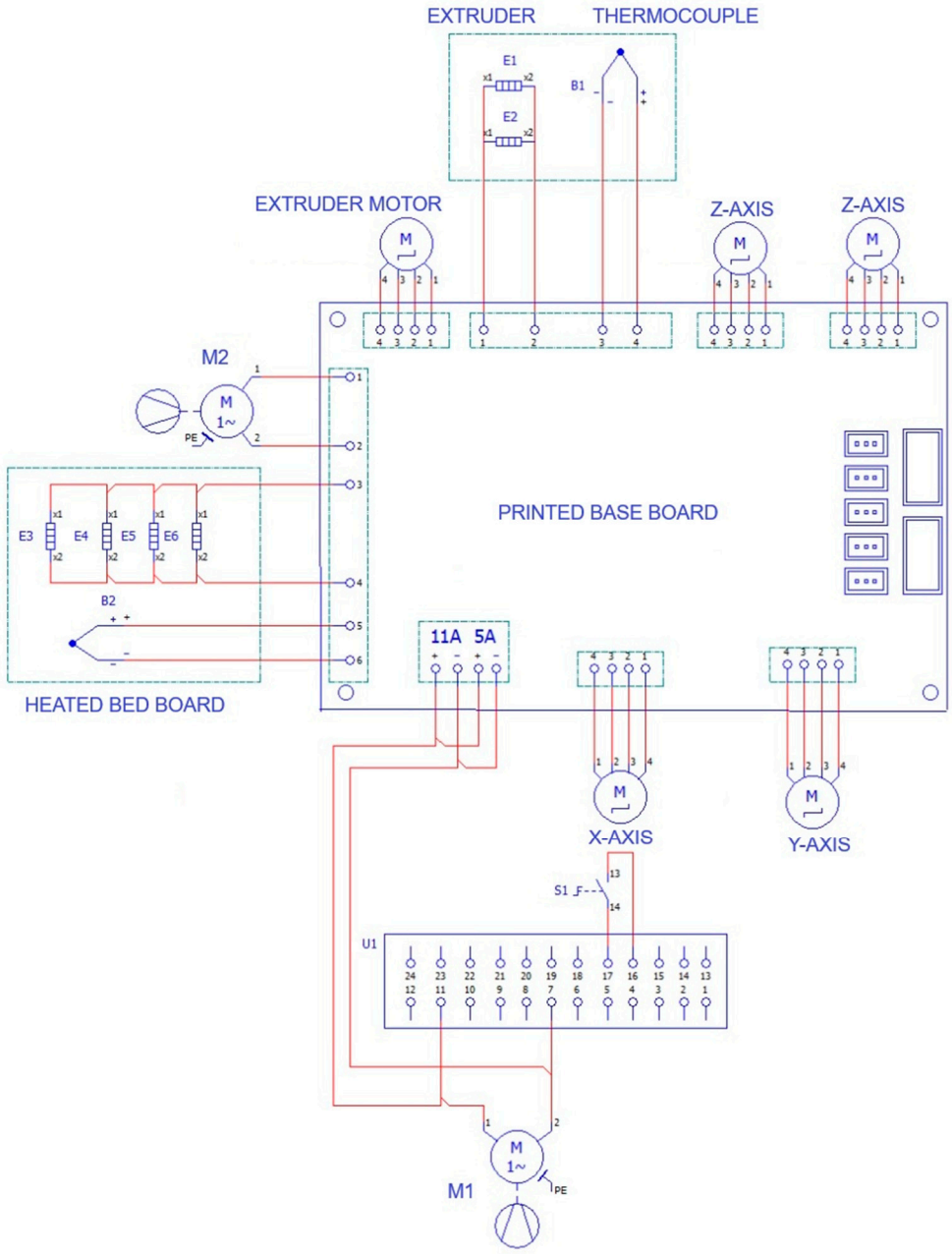

Figure 6. Electrical wiring diagram of the control and power subsystems. Annotated schematic showing the Printed Base Board, stepper-motor connectors, extruder heater and thermocouple inputs, heated-bed circuit, auxiliary connector J1, and the main 11A/5A power-supply rails.

Regarding the main connections, the stepper motors for the X, Y, Z axes and the extruder are connected to the dedicated outputs of the RAMPS 1.4 shield, which manage PWM signals. The endstop sensors are connected to the X-min, Y-min, and Z-min inputs, using a normally closed (NC) configuration for enhanced safety. The extruder thermistor is connected to the analogue input T0, while the heating resistor is connected to the digital output D10. The cooling fan is connected to D9, also configured as a PWM output. The LCD control panel and encoder are connected via the EXP1 and EXP2 ports, using SPI communication and digital signals. The SD card is accessed through the SDRAMPS

module, and the ATX power supply is connected directly to the VMOT and GND terminals of the RAMPS, providing 12 V DC.

The electronic components were mounted on a 1.5 mm thick stainless-steel tray, specifically designed to house the power supply, Arduino Mega 2560 board, RAMPS 1.4 shield, Pololu A4988 drivers, cooling fan, and input/output connectors. This tray was fixed to the main structure using M6 screws and T-slot nuts, allowing for an organised and accessible layout for maintenance. The power supply used was a 12 V, 750 W ATX unit, modified for standalone operation by bridging the PS-ON and GND pins on the Molex connector. Four output lines were selected (two 12 V and two GND) to power the RAMPS 1.4 shield directly, using tubular terminals to ensure a secure and stable connection. Figure 7a shows the ATX 12 V power supply mounted on the stainless-steel electronics tray, illustrating its physical orientation, ventilation outlet and AC-input interface. This view clarifies the mechanical integration of the power unit and its role as the primary source for the 11 A and 5 A power rails used in the RAMPS board.

The Arduino Mega 2560 board was fixed to the tray using metal spacers and M2.5 screws, onto which the RAMPS 1.4 shield was mounted. The A4988 drivers were installed in their respective sockets, ensuring correct orientation of control and power pins. Figure 7b shows the RAMPS 1.4 shield mounted on the Arduino Mega 2560, together with the installed A4988 driver modules and the power-input terminal block. This view clarifies the physical layout of the control electronics as assembled on the stainless-steel tray, supporting the reproducibility of the installation described in this section.

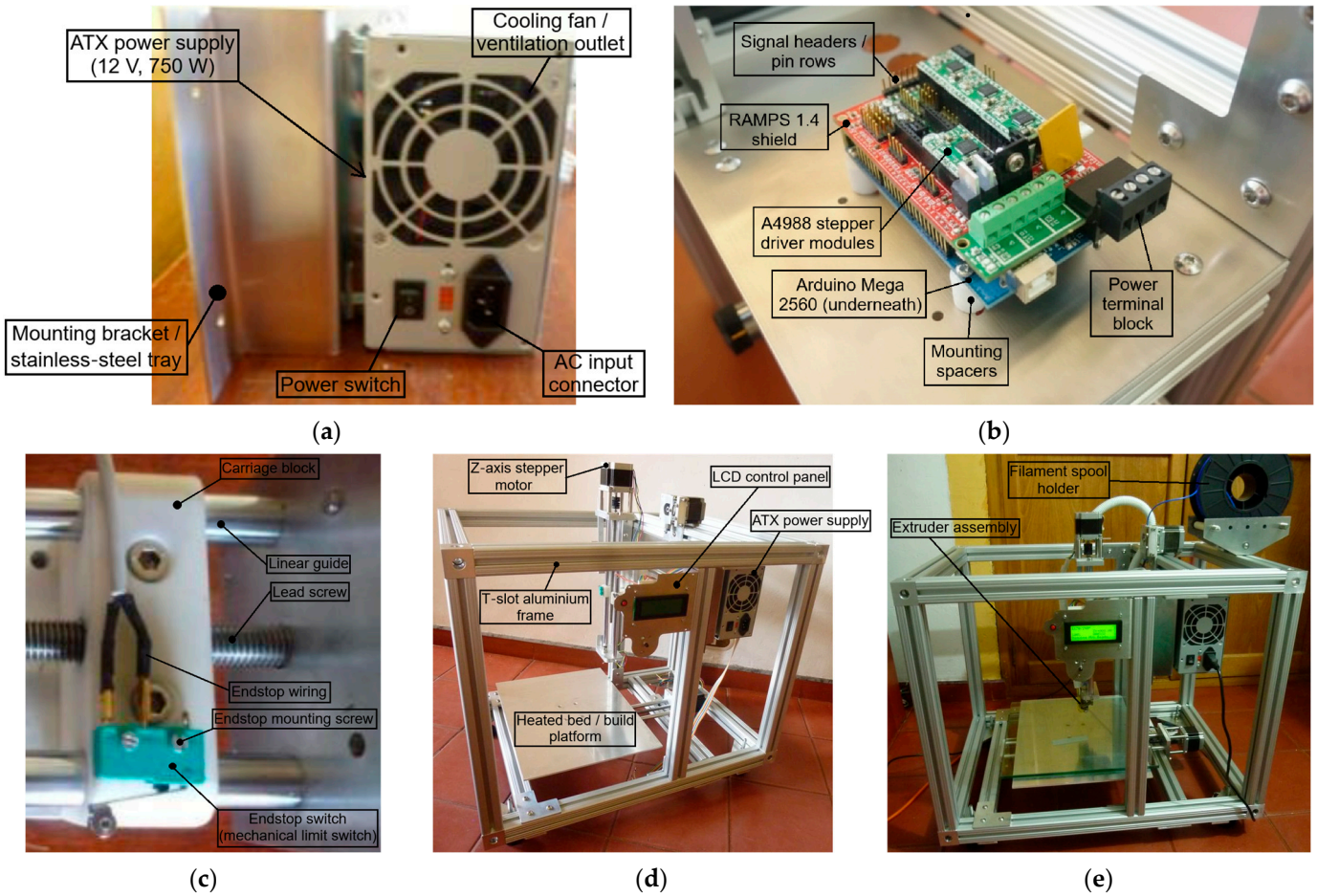

Figure 7. Final system assembly with highlighted components: (**a**) ATX 12 V power supply mounted on the stainless-steel electronics tray, showing the ventilation outlet, AC input and power switch; (**b**) RAMPS 1.4 shield mounted on the Arduino Mega 2560, showing the A4988 driver modules, power-input terminal block and signal headers; (**c**) mechanical endstop mounted on the carriage

block, showing the switch, wiring, mounting screw, linear guides and lead screw; (**d**) overview of the fully assembled electronics and frame, showing the LCD control panel, ATX power supply, Z-axis motor, heated bed and modular T-slot structure; (**e**) fully assembled 3D printer in operational configuration, showing the filament spool holder.

Once the boards were mounted, the NEMA 23 stepper motors were connected. The motor coils were identified using resistance measurements with a multimeter, and four-pin JUMPER terminals were soldered to facilitate connection to the RAMPS 1.4 shield. The cables were routed through cable glands and channels attached to the frame profiles, minimising interference and maintaining system order.

Endstop sensors were installed on each axis (X, Y, Z) in a normally closed (NC) configuration, connected to the X-min, Y-min, and Z-min pins of the RAMPS. Shielded cables with FASTON terminals and two-pin female connectors were used. Continuity of each connection was verified with a multimeter before powering the system. Figure 7c shows the installation of a mechanical endstop on the carriage block, highlighting the switch, wiring, mounting screw and its alignment with the linear guides and lead screw. This view supports the description of the endstop-installation procedure and clarifies the physical arrangement required for reliable axis homing.

The extruder was connected via a four-pin aerial terminal, allowing quick disassembly for maintenance. An extension was fabricated using JUMPER connectors for the thermistor and tubular terminals for the heating resistor, connected to the T0 and D10 pins, respectively.

Finally, the control panel, consisting of a 4 × 16 LCD screen, a rotary encoder, and a reset button, was connected. The screen was wired using jumpers for power and backlight pins, while the encoder was mounted on a universal board and connected to the RAMPS via a three-wire extension. The reset button was connected with a two-wire extension and fixed to the front panel. This set of connections enabled autonomous operation of the printer, as well as control via interface software such as CURA and Pronterface. The modularity of the design facilitates future expansions, such as the integration of multiple extruders or additional sensors. Figure 7d provides an overview of the fully assembled electronic subsystem integrated into the modular T-slot frame, showing the mounted LCD control panel, ATX power supply, Z-axis motors and the overall spatial arrangement of the wiring and mechanical interfaces. This complete view complements the detailed component-level images presented previously and supports the reproducibility of the assembly process described in this section.

3.2. Final System Assembly

The final assembly, illustrated in Figures 7 and 8, involved the physical integration of all components and the validation of practical aspects related to the modular design. The use of T-slot aluminium profiles proved advantageous for initial alignment and component positioning. However, it required careful planning to insert T-nuts into the slots beforehand, as retrofitting them later would necessitate partial disassembly, an important consideration for future iterations. The installation of the Y and Z axis carriages and the integration of the X-axis with the base plate are shown in Figure 8a,b. Figure 8a shows the assembled Y–Z carriage structure, illustrating the alignment of the linear guides and the integration of the lead-screw mechanism within the modular frame. Figure 8b shows the assembly of the X-axis subsystem, including the print-bed support plate, X-axis stepper motor, linear guides and carriage block. This view supports the description of the initial stages of the final assembly process. During this phase, it became evident that verifying the smooth movement of the linear guides before securing the side plates was essential to avoid friction and misalignment. Additionally, the coupling between leadscrews and

stepper motors, while functional, required fine adjustments to compensate for minor misalignments, reinforcing the importance of using flexible couplings.

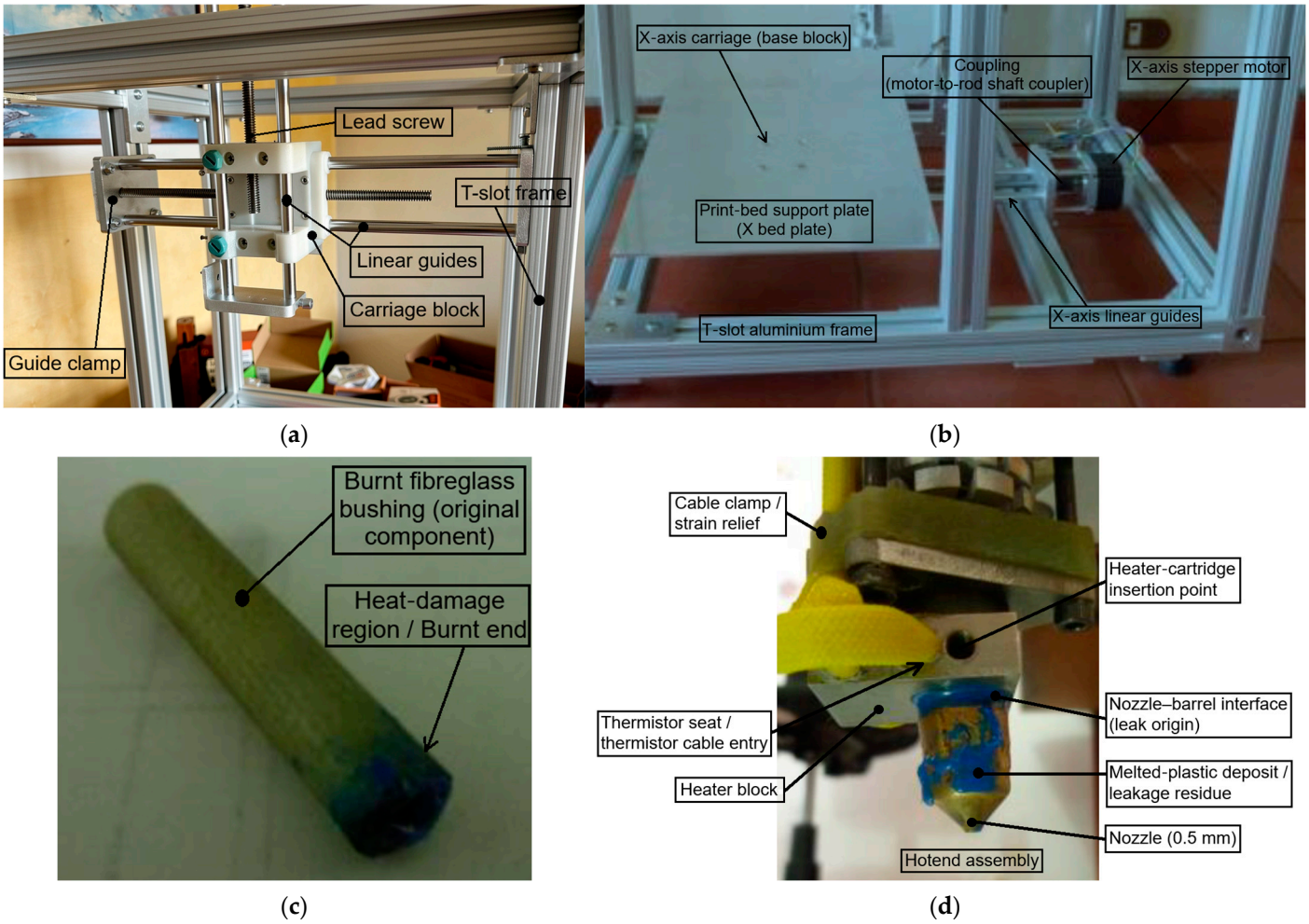

Figure 8. Assembly process and some identified issues: (**a**) assembled Y–Z carriage showing the carriage block, linear guides, lead-screw transmission and guide supports within the modular T-slot frame; (**b**) X-axis assembly showing the print-bed support plate, X-axis stepper motor, linear guides and T-slot frame integration; (**c**) burnt fibreglass bushing removed from the hotend, showing the heat-damage region that caused excessive friction and filament clogging; (**d**) nozzle leakage showing molten-plastic accumulation at the interface between the nozzle and the threaded barrel, indicating insufficient sealing at the heater-block junction.

Several mechanical issues were observed during the assembly process:

- Filament feeding system slippage: The spring-loaded tension mechanism initially caused gear slippage, reducing effective extrusion. This issue was resolved by replacing the original springs (Ø 6 mm, 18 mm length) with stiffer ones, increasing compression force by approximately 30%. The improvement is shown in Figure 5a.
- Inadequate bushing in the extruder: The original fibreglass bushing in the hotend generated excessive friction, leading to clogs and inconsistent filament flow. Figure 8c shows the original fibreglass bushing removed from the hotend, where the burnt end and surface degradation are clearly visible. This damage was responsible for excessive friction and clogging during filament feeding. It was replaced with a PTFE bushing (friction coefficient ≈ 0.04), which reduced resistance by 60% and stabilised extrusion and improved extrusion consistency.

- Nozzle leakage: Material leakage was observed at the junction between the nozzle and the threaded barrel, affecting surface quality. The issue, illustrated in Figure 8d, was resolved by applying high-temperature silicone sealant and tightening the joint to 2.5 N·m, eliminating the leak and improving surface finish.

The electronic components were mounted on a custom-designed 1.5 mm thick stainless-steel tray, which housed the ATX power supply (12 V, 750 W), Arduino Mega 2560 board, RAMPS 1.4 shield, A4988 drivers, cooling fan, and I/O connectors. The tray was secured to the frame using M6 screws and T-slot nuts, ensuring a stable and accessible layout. Cable routing was managed using adhesive cable ducts and cable glands fixed to the frame, which helped minimise electromagnetic interference and maintain system order.

The installation of the control panel, comprising a 4 × 16 LCD screen, rotary encoder, and reset button, also required careful cable management to prevent interference with axis movement. The modular layout facilitated these adjustments and is recommended for future designs aiming for ease of maintenance and expandability.

Figure 7e shows the 3D printer fully assembled in its operational configuration, including the mounted filament spool, LCD interface, Z-axis motors, heated bed and final cable-routing arrangement. This complete view illustrates how all mechanical, electronic and control subsystems integrate within the modular T-slot frame, complementing the assembly description provided in this section. These observations highlight the importance of anticipating assembly constraints in modular designs and provide practical insights for users aiming to replicate or adapt the system in educational or low-resource settings.

3.3. Functional Testing

Once the assembly was completed, initial tests were conducted to verify the operability of the system. These tests allowed for the evaluation of axis movement, sensor response, thermal stability of the extruder, and communication with the control software. They also enabled the adjustment of critical parameters and confirmed the overall stability of the system.

3.3.1. Movement of X, Y, Z Axes

Axis movement was tested using manual commands via the control interface (see Figure 4c). The direction of movement was validated and corrected through firmware parameters. Movements of 10 mm were commanded and measured using a digital calliper, yielding deviations of less than ±0.2 mm from the nominal value. The homing speed was configured in the firmware as HOMING_FEEDRATE {2000, 2000, 160, 0} mm/min for the X, Y, and Z axes, respectively. This adjustment ensured fast positioning without compromising accuracy. Smooth motion was achieved after minor adjustments to guide tension and leadscrew alignment. This verification is essential to ensure precision in material deposition.

3.3.2. Endstop Activation

The correct operation of the endstops was validated during the homing process. Activation logic was adjusted in the firmware (e.g., X_ENDSTOPS_INVERTING = true) to prevent collisions and ensure repeatable positioning. The tests confirmed positioning repeatability with a tolerance of less than ±0.1 mm.

3.3.3. Extruder Temperature Control

The thermal system was tested by increasing the hotend temperature from 70 °C to 190 °C for PLA printing. Thermistor readings were compared with external measurements using a thermocouple, showing deviations of less than ±2 °C, thereby validating the stability of the PID control. The stabilisation time at 190 °C was approximately 3 min. This control is critical to prevent extrusion failures.

3.3.4. Communication with CURA and Pronterface Software

Communication between the Marlin firmware and CURA software was verified via USB connection at 115,200 baud using a serial protocol. Correct interpretation of G-code and synchronisation with the hardware were confirmed. Additionally, Pronterface was used for specific extrusion tests and parameter adjustments.

3.4. System Calibration

Calibration was carried out to ensure dimensional accuracy and stability throughout the printing process. The procedures described in the methodology were applied iteratively, and the results are summarised below.

3.4.1. Firmware Adjustment (Steps per Unit, Travel Limits, Axis Direction)

Critical parameters were configured in the Configuration.h file of the Marlin firmware. The initial values for steps per unit were DEFAULT_AXIS_STEPS_PER_UNIT {1958, 1958, 2148, 98} corresponding to the X, Y, Z axes and the extruder, respectively.

A command was issued to extrude 100 mm of filament, and 86 mm were measured, indicating a 14% error. This calibration of steps per unit [steps/mm] is a critical stage in the setup of a 3D printer, ensuring that movements commanded from the control software correspond to the actual physical displacements of the machine. The detected error was corrected using a proportional calculation, adjusting the extruder value from 98 to 714.28 steps/mm. This procedure was repeated for each axis, including the extruder, whose calibration is essential to prevent over-extrusion or under-extrusion.

Travel limits were set as follows: X_MAX_POS = 300 mm; Y_MAX_POS = 300 mm; Z_MAX_POS = 180 mm; to prevent collisions. Axis directions were verified and adjusted using the firmware variables INVERT_X_DIR, INVERT_Y_DIR, and INVERT_Z_DIR.

3.4.2. Bed Levelling

The print bed was levelled using a 5 mm glass plate placed on the base platform (see Figure 7). The extruder height was adjusted to maintain a uniform gap of 0.10 mm at all four corners, validated using a digital calliper. This adjustment is critical to ensure proper first-layer adhesion and to prevent warping.

3.4.3. Filament Feed System Calibration

Following the previously identified 14% error, the steps per unit parameter was adjusted, and the test was repeated, yielding 99.5 mm—within a tolerance of ±0.5 mm. Additionally, the tension of the feeding system was reinforced by replacing the springs, reducing gear slippage (see Figure 5a).

3.4.4. Thermal Stability Validation

The hotend temperature was tested at 70 °C and 190 °C for PLA printing. Thermistor readings were compared with external thermocouple measurements, showing deviations of less than ±2 °C. The system reached thermal stability at 190 °C within 3 min, confirming the effectiveness of the PID control.

3.5. Printing Results

Following the completion of calibration, printing tests were conducted to evaluate dimensional accuracy, layer adhesion, and system stability. Results were compared before and after calibration, using both simple and complex geometries. The dimensional values reported correspond to single-print measurements intended to verify functional calibration rather than statistical variability.

3.5.1. Initial Prints Without Calibration

The first printed parts were a square-based prism measuring 20 × 20 × 2 mm and a cylinder of Ø25 mm × 3 mm. Significant deviations were observed in the cube, with actual dimensions of 21.8 mm in X, 19.2 mm in Y, and 2.05 mm in Z, representing an average error of +6.5%. Figure 9a shows the initial test prints obtained before calibration, where several defects are evident, including under-extrusion, poor first-layer adhesion, blob formation and warping. These issues reflect the lack of synchronisation between extrusion parameters, bed levelling and axis motion, and justify the calibration procedures described in the following sections. The cylinder measured 26.4 mm in diameter, corresponding to an error of +5.6%, visible in Figure 9b that shows the cylindrical test piece printed before calibration, exhibiting severe extrusion inconsistencies, surface roughness, edge deformation, and first-layer irregularities. These defects highlight the lack of synchronisation between extrusion flow, bed levelling, and axis motion, reinforcing the need for the calibration procedures described in the following section.

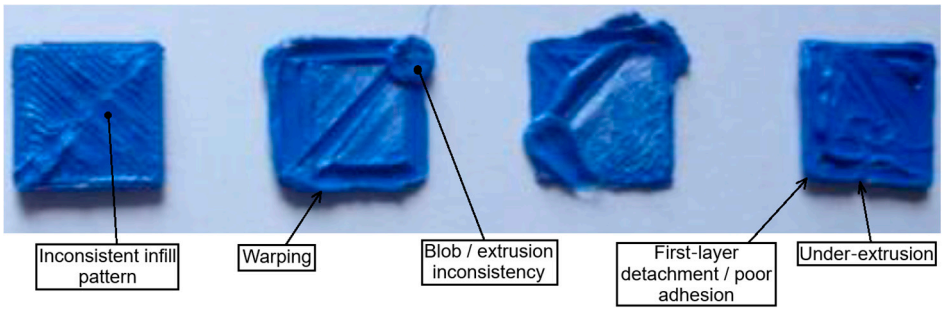

(**a**)

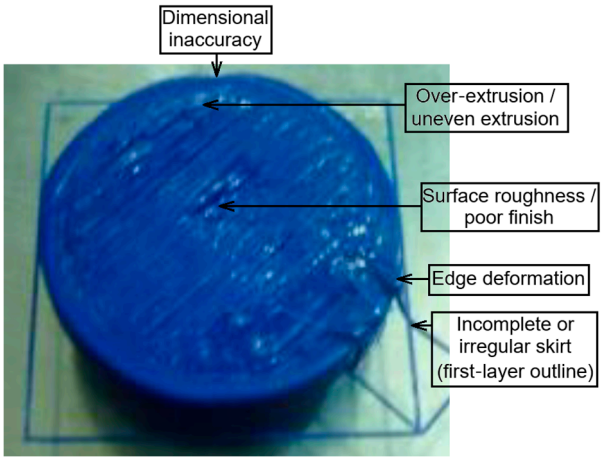

(**b**)

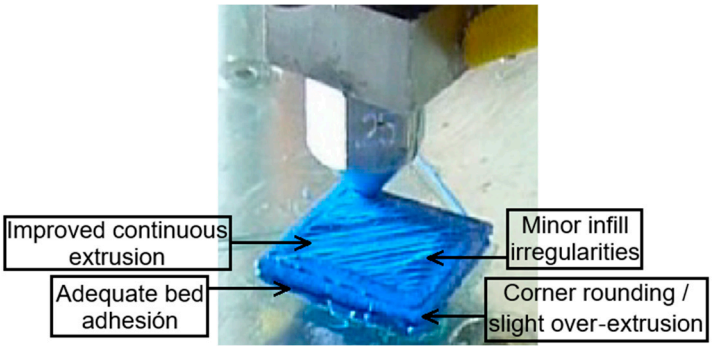

(**c**)

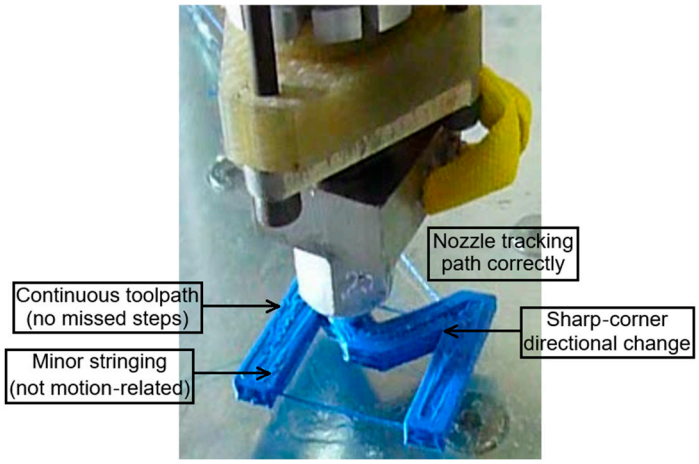

(**d**)

Figure 9. Printing results: (**a**) initial prints without calibration showing under-extrusion, first-layer detachment, blob formation and warping; (**b**) cylindrical test piece printed before calibration, showing over-extrusion, surface roughness, edge deformation and first-layer irregularities; (**c**) thin-wall test printed after calibration, showing improved extrusion continuity and bed adhesion, with minor surface irregularities still present; (**d**) post-calibration motion-validation print ("M" path), showing correct axis synchronisation and continuous toolpath execution, with minor non-critical stringing.

3.5.2. Prints After Calibration

After adjusting the steps per unit and levelling the bed, the same geometries were reprinted. The cube now measured 20.1 mm in X, 20.0 mm in Y, and 2.02 mm in Z, reducing the average error to +0.5%. Figure 9c the thin-wall test performed after the mechanical and firmware calibration procedures. The print quality improved substantially compared to the initial results, exhibiting continuous extrusion, proper bed adhesion and the absence of severe defects such as warping or material blobs. Nevertheless, minor irregularities remain visible in the infill pattern and surface finish, reflecting the non-optimised nature of this prototype and the fact that the calibration process focused on achieving functional performance rather than fine-tuned quality optimisation. Compared to the prints shown in Figure 9a, where severe under-extrusion, detachment and deformation were present, Figure 9c demonstrates a clear improvement in print consistency following the calibration process. The cylinder measured 25.1 mm in diameter, with an error of +0.4% (see Figure 5b). Surface quality improved significantly, with uniform layers and complete infill. The corrected E-steps value remained stable throughout the subsequent calibration and test-print sessions, with no additional drift observed during operation.

3.5.3. Complex Geometry Prints

Figure 9d shows a motion-validation test carried out after calibration, in which the extruder follows a sharp directional pattern ("M" shape) without missed steps or positional drift. The continuous deposition along the angled segments confirms that the X- and Y-axis movements are properly synchronised and that the step-per-unit calibration ensures stable motion. Although minor artefacts such as slight stringing remain visible, these do not compromise the assessment of motion stability, which was the primary purpose of this test. The parts exhibited good edge definition and dimensional stability, confirming the effectiveness of the calibration. The average printing time for these parts was 45 min, using the following parameters: layer height: 0.25 mm; infill: 20%; the motion parameters used during validation were 50 mm/s print speed, 3000 mm/s^2 acceleration and a jerk setting of 20 mm/s, consistent with typical RepRap-class configurations.

4. Discussion

The results obtained in this study confirm the initial hypothesis: it is possible to build a functional, accurate, and replicable 3D printer using exclusively accessible components and open-source technologies. The reduction in average dimensional error from over 6% to less than 0.5% following calibration, along with improvements in surface quality and thermal stability, validates the technical feasibility of the proposed system. The dimensional accuracy obtained after calibration (average error below 0.5%) is consistent with the ranges reported for other low-cost or RepRap-based FDM systems. Minetola et al. (2018) observed improvements that brought Prusa i3 printers close to ISO IT7–IT8 accuracy classes [13], while Rendón-Medina et al. (2018) reported dimensional errors of approximately 1.96% in clinical-grade low-cost printers [14]. Similarly, Khan et al. (2025) reported geometric deviations up to 3.3% prior to parameter optimisation [5]. In this context, the post-calibration behaviour of our prototype aligns with the performance envelope of comparable open-source machines, despite relying exclusively on accessible components and simple calibration procedures. The motion-validation results shown in Figure 9d further indicate that axis synchronisation and extrusion stability reach levels suitable for educational and prototyping applications, even without the advanced optical or closed-loop methods described in recent metrological studies.

From the perspective of previous studies, these findings complement and extend the approaches documented by authors such as Schuh (2024) [10] and Khan et al. (2025) [5], who explored the construction of low-cost FFF printers but did not detail systematic calibration procedures or fault-resolution strategies. Likewise, the observations of Keller et al. (2025) [6] and Jadayel (2024) [7] regarding the importance of precise calibration to reduce systematic errors are reinforced here. However, this study demonstrates that such improvements can be achieved without resorting to advanced optical or computational systems, but rather through mechanical adjustments and accessible firmware.

The modular design, based on T-slot profiles and an Arduino–RAMPS architecture, not only facilitated assembly and maintenance but also enabled an organised integration of mechanical, electronic, and control subsystems. This modular approach aligns with the recommendations of Kechagias et al. (2022) [18] concerning the need for systematic methodologies to control critical parameters in the FFF process.

The issues identified—such as gear slippage, inadequate bushings, and nozzle leakage—were addressed through practical solutions that can be replicated by non-specialist users. These interventions demonstrate that system reliability does not depend solely on hardware, but also on the ability to identify and resolve faults through technical observation and iterative adjustments.

In the broader context of additive manufacturing, this work provides empirical evidence supporting the democratisation of prototyping technologies through open hardware. As suggested by Gwamuri et al. (2016) [11] and Dupont et al. (2021) [26], technological appropriation in low-resource communities requires not only economic access but also clear and replicable technical documentation, as presented in this article.

Future research directions could include the incorporation of feedback sensors for closed-loop control, the development of interchangeable modules for multi-material printing, and the integration of alternative energy systems such as solar power. Additionally, it is recommended to explore the use of recycled or biocomposite materials as printing feedstock, in line with the sustainable approaches proposed by Campana et al. (2021) [25].

5. Limitations

The scope of this study is strictly centred on the engineering development and functional validation of a single prototype. It does not attempt to propose new design theories or optimisation mechanisms, nor does it pursue experimental generalisation beyond the documented implementation. Future studies could extend this work through comparative performance benchmarking or advanced modelling-based optimisation, which fall outside the development-focused remit of the present contribution. Additionally, no comparative evaluation against commercial or open-source printers was conducted, as the aim of the study was functional validation of the prototype rather than performance benchmarking.

A theoretical error model or nonlinear extrusion analysis was not included, as the aim of the study was functional calibration of a development-stage prototype. The proportional method provides sufficient accuracy for verifying operability without requiring full characterisation of thermal, rheological or mechanical parameters. No statistical analysis (such as standard deviations or confidence intervals) is reported because this study did not involve multiple replicates or an experimental design aimed at quantifying variability. The objective was to verify functional operation of a development-stage prototype rather than to conduct metrological or performance-variability assessment.

6. Conclusions

This work documents the design, construction, calibration, and fault resolution of a low-cost modular 3D printer based on open-source technologies, validating the hypothesis that it is possible to develop a functional and replicable system using exclusively accessible components. The results obtained, both in axis movement tests and print quality, demonstrate that the modular approach and the use of open-source hardware and software platforms enable levels of precision suitable for educational and prototyping applications.

The methodology that was employed, which integrates CAD modelling, electronic integration, firmware configuration and iterative calibration, provides a replicable guide for similar projects in resource-constrained contexts. Furthermore, the identification and resolution of mechanical and thermal faults offer practical recommendations that may be useful for non-specialist users.

Taken together, this study contributes to the democratisation of additive manufacturing, reinforcing the value of open hardware as a tool for education, innovation, and technological appropriation. It is recommended that future research should explore the incorporation of closed-loop control, multi-material printing, and the use of recycled or biocomposite materials, thereby expanding the technical, social, and environmental impact of such developments.

Beyond its technical validation, the developed machine has potential impact across several domains. In educational settings, its low cost, modularity and open-source configuration offer a practical platform for teaching engineering concepts related to automation, CAD, electronics and control. For researchers, the system provides a fully documented and reproducible tool that can be adapted for experimental prototyping, instrumentation or process-monitoring studies. In low-resource or rural environments, the accessibility of materials and the detailed assembly procedures presented here contribute to the democratisation of digital fabrication, enabling local technological appropriation. Finally, for small enterprises and industry, the printer represents a viable entry-level solution for rapid prototyping and customised manufacturing workflows, reinforcing the relevance of open hardware in emerging innovation ecosystems.

Author Contributions: Conceptualisation, J.G.A.-M. and L.M.N.-G.; methodology, M.A.M.-G.; software, M.A.M.-G.; validation, M.A.M.-G., J.G.A.-M. and L.M.N.-G.; formal analysis, M.A.M.-G.; investigation, M.A.M.-G. and J.G.A.-M.; resources, M.A.M.-G., J.G.A.-M. and L.M.N.-G.; data curation, M.A.M.-G.; writing—original draft preparation, M.A.M.-G. and J.G.A.-M.; writing—review and editing, J.G.A.-M. and L.M.N.-G.; visualisation, M.A.M.-G.; supervision, J.G.A.-M.; project administration, L.M.N.-G.; funding acquisition, M.A.M.-G., J.G.A.-M. and L.M.N.-G. All authors have read and agreed to the published version of the manuscript.

Funding: This research received no external funding. The Article Processing Charge (APC) was covered by the authors.

Data Availability Statement: A public GitHub repository has been created to provide open access to the core resources associated with the developed 3D printer. The repository includes the Marlin firmware (MarlinFirmware Project, GitHub Open-Source Community, USA) folder, the design files, and the AGPL-3.0 open-source licence, and is available at: https://github.com/mauricioamg26/Impresora-3d (accessed on 5 February 2026).

Acknowledgments: The authors would like to express their gratitude to the Universidad de Valladolid, Universidad Surcolombiana, Instituto Tecnológico Metropolitano (ITM), and Fundación Carolina for providing the academic, technical and institutional support that enabled the development of this work. Their collaboration was essential throughout the project. During the preparation of this manuscript, the authors used Microsoft Copilot (GPT-4 architecture, Microsoft Corporation, Redmond, WA, USA) for drafting and refining specific sections of the text and AI-powered inpainting tools from OpenArt (OpenArt AI, San Francisco, CA, USA) to enhance resolution and legibility of some images. The authors have reviewed and edited the output and take full responsibility for the content of this publication.

Conflicts of Interest: Authors Mauricio Arturo Moreno-Gerena was employed by the SIMEX S.A.S. The remaining authors declare that the research was conducted in the absence of any commercial or financial relationships that could be construed as a potential conflict of interest.

Abbreviations

The following abbreviations are used in this manuscript:

3D	Three-Dimensional
ATX	Advanced Technology eXtended
CAD	Computer-Aided Design
DIY	Do It Yourself
FDM	Fused Deposition Modelling
FFF	Fused Filament Fabrication
HMI	Human–Machine Interface
IDE	Integrated Development Environment
LCD	Liquid Crystal Display
NC	Normally Closed
PID	Proportional–Integral–Derivative
PLA	Polylactic Acid
PTFE	Polytetrafluoroethylene
RAMPS	RepRap Arduino Mega Pololu Shield
SD	Secure Digital
SPI	Serial Peripheral Interface
USB	Universal Serial Bus

References

1. Marín, J.G.A. *Evaluación Preliminar del Potencial de la Manufactura por Capas para la Industria Colombiana*; Universidad Nacional de Colombia: Medellín, Colombia, 2007.
2. Anzalone, G.C.; Zhang, C.; Wijnen, B.; Sanders, P.G.; Pearce, J.M. A low-cost open-source metal 3-D printer. *IEEE Access* **2013**, *1*, 803–810. https://doi.org/10.1109/ACCESS.2013.2293018.
3. Weiss, J.D.; Mermin-Bunnell, A.; Solberg, F.S.; Tam, T.; Rosalia, L.; Sharir, A.; Rütsche, D.; Sinha, S.; Choi, P.S.; Shibata, M.; et al. A Low-Cost, Open-Source 3D Printer for Multimaterial and High-Throughput Direct Ink Writing of Soft and Living Materials. *Adv. Mater.* **2025**, *37*, e2414971. https://doi.org/10.1002/adma.202414971.
4. Laplume, A.; Anzalone, G.C.; Pearce, J.M. Open-source, self-replicating 3-D printer factory for small-business manufacturing. *Int. J. Adv. Manuf. Technol.* **2016**, *85*, 633–642. https://doi.org/10.1007/s00170-015-7970-9.
5. Khan, I.; Abas, M.; Ahmad, S.; Al Rashid, A.; Koç, M. Fabrication of a low-cost fused filament fabrication-based 3D printer and investigation of the effects of process parameters on mechanical properties of 3D-printed samples. *J. Eng. Res.* **2025**, *13*, 1936–1946. https://doi.org/10.1016/j.jer.2024.06.018.
6. Keller, W.; Girard, J.; Goldberg, M.W.; Zhang, S. Precise calibration for error detection and correction in material extrusion additive manufacturing using digital fringe projection. *Meas. Sci. Technol.* **2025**, *36*, 025203. https://doi.org/10.1088/1361-6501/ada847.
7. Jadayel, M. *Improving Geometric Accuracy of Fused Filament Fabrication (FFF) 3D Printed Parts by Computational Analysis of Digitized Sacrificial Parts*; Polytechnique Montréal: Montreal, QC, Canada, 2024. Available online: https://publications.polymtl.ca/59432/ (accessed on 25 August 2025).
8. Ahmad, M.N.; Tarmeze, A.A.; Rasib, A.A. Capability of 3D printing technology in producing molar teeth prototype. *Int. J. Eng. Appl.* **2020**, *8*, 64–70. https://doi.org/10.15866/irea.v8i2.17949.
9. Wittbrodt, B.T.; Glover, A.G.; Laureto, J.; Anzalone, G.C.; Oppliger, D.; Irwin, J.L.; Pearce, J.M. Life-cycle economic analysis of distributed manufacturing with open-source 3-D printers. *Mechatronics* **2013**, *23*, 713–726. https://doi.org/10.1016/j.mechatronics.2013.06.002.
10. Schuh, J.F. *Building a Low-Cost 3D Printer*; Regional University of Blumenau: Blumenau, Brazil, 2024.
11. Gwamuri, J.; Poliskey, J.E.; Pearce, J.M. Open-source 3D printers: An appropriate technology for building low-cost optics labs for the developing communities. In Proceedings of the 14th Conference on Education and Training in Optics and Photonics, ETOP 2017, Hangzhou, China, 29–31 May 2017; p. 187. https://doi.org/10.1117/12.2269852.
12. Petersen, E.E.; Pearce, J. Emergence of Home Manufacturing in the Developed World: Return on Investment for Open-Source 3-D Printers. *Technologies* **2017**, *5*, 7. https://doi.org/10.3390/technologies5010007.
13. Minetola, P.; Galati, M.; Iuliano, L.; Atzeni, E.; Salmi, A. The Use of Self-replicated Parts for Improving the Design and the Accuracy of a Low-cost 3D Printer. *Procedia CIRP* **2018**, *67*, 203–208. https://doi.org/10.1016/j.procir.2017.12.200.
14. Rendón-Medina, M.A.; Andrade-Delgado, L.; Telich-Tarriba, J.E.; Fuente-Del-Campo, A.; Altami-rano-Arcos, C.A. Dimensional error in rapid prototyping with open-source software and low-cost 3D-printer. *Plast. Reconstr. Surg. Glob. Open* **2018**, *6*, e1646. https://doi.org/10.1097/GOX.0000000000001646.
15. Rosli, N.A.; Alkahari, M.R.; Ramli, F.R.; Maidin, S.; Sudin, M.N.; Subramoniam, S.; Furumoto, T. Design and development of a low-cost 3d metal printer. *J. Mech. Eng. Res. Dev.* **2018**, *41*, 47–54. https://doi.org/10.26480/jmerd.03.2018.47.54.
16. Sood, R.; Pradhan, S.K. Design and development of a low-cost open-source 3D printer and its single response optimization using polylactic acid (PLA) material. *Mater. Today Proc.* **2019**, *27*, 2981–2991. https://doi.org/10.1016/j.matpr.2020.04.905.
17. Nath, P.; Olson, J.D.; Mahadevan, S.; Lee, Y.T.T. Optimization of fused filament fabrication process parameters under uncertainty to maximize part geometry accuracy. *Addit. Manuf.* **2020**, *35*, 101331. https://doi.org/10.1016/j.addma.2020.101331.
18. Kechagias, J.; Chaldas, D.; Vidakis, N.; Salonitis, K.; Vaxevanidis, N.M. Key parameters controlling surface quality and dimensional accuracy: A critical review of FFF process. *Mater. Manuf. Process.* **2022**, *37*, 963–984. https://doi.org/10.1080/10426914.2022.2032144.
19. Erokhin, K.S.; Naumov, S.A.; Ananikov, V.P. Defects in 3D Printing and Strategies to Enhance Quality of FFF Additive Manufacturing. A Review. *ChemRxiv* **2023**, 1–29. https://doi.org/10.26434/chemrxiv-2023-lw1ns.
20. Weiss, B.M. Closed-Loop Control of a 3D Printer Gantry. *J. Chem. Inf. Model.* **2013**, *53*, 1689–1699.
21. Ctibor, J.; Pazdera, I. The New Stepper Driver for Low-Cost Arduino Based 3D Printer with Dynamic Stepper Control. In *Advances in Intelligent Systems and Computing: Mechatronics 2017*; Březina, T., Jabłoński, R., Eds.; Springer International Publishing: Cham, Switzerland, 2018; pp. 458–466. https://doi.org/10.1007/978-3-319-65960-2_57.

22. Salazar-Serrano, L.J.; Jiménez, G.; Torres, J.P. How to automate a kinematic mount using a 3D printed arduino-based system. *Inventions* **2018**, *3*, 39. https://doi.org/10.3390/inventions3020039.
23. Praja, P.; Kanna, R.R.; Bazeer, E.; Arunpandiyan, S. *Design and Fabrication of FDM Based Portable 3D Printer*; Anna University: Chennai, India, 2020.
24. Khona, N.B. Design and Fabrication of Arduino Based Flexible Manufacturing Process on the Desk: 3D Printing. *Int. J. Res. Appl. Sci. Eng. Technol.* **2022**, *10*, 2603–2610. https://doi.org/10.22214/ijraset.2022.44427.
25. Campana, G.; Mele, M.; Ciotti, M.; Rocchi, A. Environmental impacts of self-replicating three-dimensional printers. *Sustain. Mater. Technol.* **2021**, *30*, e00335. https://doi.org/10.1016/j.susmat.2021.e00335.
26. Dupont, L.; Fedoua, K.; Pearce, J.M.; Ortt, R.J. 'Do-It-Together': Towards the Factories of the Future. In *Cosmolocal Reader*; Ramos, J.M., Bauwens, M., Ede, S., Wong, J.G., Eds.; Futures Lab: Atlanta, GA, USA, 2021; pp. 52–59.
27. Masa, A.T.; Ramos, R.A.R.; Recto, K.H. Impacts of Open-source Hardware Movements on Electronics Engineering Educational Outcomes. *Inst. Electron. Eng. Philipp. J.* **2024**, *6*, 1–7.
28. Seidle, A.G.; Pearce, J.M. Overcoming Limitations of Proprietary Scientific Hardware Funding. *J. Knowl. Econ.* **2025**, 1–18. https://doi.org/10.1007/s13132-025-02783-w.
29. Hallgren, J.; Wiberg, W. *Open Source Hardware: A Case Study of Userdeveloped Derivatives*; The Royal Institute of Technology: Stockholm, Sweden, 2015.
30. Ragab, D.; Tutunji, T.A. Mechatronic system design project: A 3D printer case study. In *Proceedings of the 2015 IEEE Jordan Conference on Applied Electrical Engineering and Computing Technologies (AEECT)*; IEEE: New York, NY, USA, 2015; pp. 1–6.
31. Veliu, C.; Petzold, V.; Reichelt, D.; Stange, M.; Ihlenfeldt, S. A case study on the use of open-source hardware in mechanical engineering. *Procedia CIRP* **2024**, *128*, 680–685. https://doi.org/10.1016/j.procir.2024.03.042.
32. Dunn, K.; Feng, C.; Peek, N. Jubilee: A case study of distributed manufacturing in an open-source hardware project. *J. Open Hardw.* **2023**, *7*, 1–15. https://doi.org/10.5334/joh.51.
33. Omer, M.; Kaiser, M.; Buxbaum-Conradi, S.; Moritz, M.; Redlich, T. Designing for replicability: A qualitative empirical study on the replication of open-source machine tools. *Des. Sci.* **2024**, *10*, e30. https://doi.org/10.1017/dsj.2024.35.
34. Kantaros, A.; Diegel, O.; Piromalis, D.; Tsaramirsis, G.; Khadidos, A.O.; Khan, F.Q.; Jan, S. 3D printing: Making an innovative technology widely accessible through makerspaces and outsourced services. In *Materials Today: Proceedings*; Elsevier Ltd.: Amsterdam, The Netherlands, 2021; pp. 2712–2723. https://doi.org/10.1016/j.matpr.2021.09.074.
35. Doloi, S.; Das, M.; Li, Y.; Cho, Z.H.; Xiao, X.; Hanna, J.V.; Osvaldo, M.; Tat, L.N.W. Democratizing self-driving labs: Advances in low-cost 3D printing for laboratory automation. *Digit. Discov.* **2025**, *4*, 1685–1721. https://doi.org/10.1039/d4dd00411f.
36. Amri, A.A.N.; Sumbodo, W. Pengembangan 3D Printer tipe core XY berbasis fused deposition modeling (FDM) menggunakan software Autodesk Inventor 2015. *J. Din. Vokasional Tek. Mesin* **2018**, *3*, 110–115. https://doi.org/10.21831/dinamika.v3i2.21407.
37. Kun, K. Reconstruction and development of a 3D printer using FDM technology. In *Procedia Engineering*; Elsevier Ltd.: Amsterdam, The Netherlands, 2016; pp. 203–211. https://doi.org/10.1016/j.proeng.2016.06.657.
38. Darsin, M.; Jatisukamto, G.; Sabri-Hussin, M. Design of Portable Cartensia 3D Printer Portable Using Arduino Mega 2560. *J. 3D Print. Addit. Manuf.* **2021**, *1*, 1–7. Available online: https://www.researchgate.net/publication/356171717 (accessed on 25 August 2025).
39. Solarte, J.; Hoyos, A.; Mercado, F.; Rojas, Á. Development of a 3D Printer with Dual Extrusion Head for Industrial Applications. *I+T+C-Res. Technol. Sci.* **2024**, *1*, 1–11. https://doi.org/10.57173/ritc.v1n18a11.
40. Oluwajobi, A.O.; Kolawole, F.O. Design of a Fused Filament Fabrication (FFF) 3D-printer. *Niger. J. Technol.* **2021**, *40*, 252–260. https://doi.org/10.4314/njt.v40i2.10.
41. Harsha-Vardhan, U.; Bhavana, K.; Vamsi, G.; Ashish, D. *Fused Deposition Modelling 3D Printer Using ARDUINO*; Anil Neerukonda Institute of Technology and Sciences: Bheemunipatnam, India, 2018.
42. Yavuz, G.A. *The Production of Objects with Three Dimensional Printing Technique*; Dokuz Eylül University: İzmir, Türkiye, 2014.
43. Moore, S.; Armstrong, P.; McDonald, T.; Yampolskiy, M. Vulnerability Analysis of Desktop 3D Printer Software. In *Proceedings of the Resilience Week (RWS), Chicago, IL, USA, 2016*; IEEE: New York, NY, USA, 2016; pp. 46–51. https://doi.org/10.1109/RWEEK.2016.7573305.
44. Karakuş, S. Design and Manufacturing of a Two-Stage Reduction Gearbox with 3D Printers. *Int. J. 3D Print. Technol. Digit. Ind.* **2023**, *7*, 18–28. https://doi.org/10.46519/ij3dptdi.1206809.
45. Altan, A.; Hacıoğlu, R. The Algorithm Development and Implementation for 3D Printers based on Adaptive PID Controller. *J. Polytech.* **2018**, *21*, 559–564. https://doi.org/10.2339/politeknik.391790.
46. Nguyen, T. *Study, Design and Implementation of 3D Printer*; Häme University of Applied Sciences: Hämeenlinna, Finland, 2019.

47. Breault, S.; Godbole, V.; Kent, J.; Tarnowski, M. Five Axis 3D Printer. University of Rhode Island: South Kingstown, Rhode Island, 2021. Available online: https://digitalcommons.uri.edu/mechanical-engineering-capstones (accessed on 25 August 2025).
48. Noorani, R.; Lynch, M.; Hodgkiss, P.; Fumo, M.; Burke, C. Design and Manufacturing of a 3D Printer for Teaching and Research. In *IOP Conference Series: Materials Science and Engineering*; Institute of Physics Publishing: Bristol, England, 2019. https://doi.org/10.1088/1757-899X/652/1/012058.
49. Sawczuk, M.G. *Design and Control of a 3D Printed, 6DoF Robot Arm*; KTH Royal Institute of Technology: Stockholm, Sweden, 2021.
50. Putra, A.K.; Fidiyanto, F.; Prakoso, B.; Armantya, R.Z.; Sandi, M.K.; Al Haris, F.H.S. Perakitan 3D printer fused deposite modeling (FDM) berbasis Arduino Mega 2560. *Gaung Inform.* **2019**, *12*, 123–133.
51. Mardiyana, D.; Sulaiman, Z.; Ihsan, S.; Ridha, F.; Rahman, T. Rancang Bangun 3D Printer FDM Model Cartesian Berbasis Arduino. *J. Mater. Dan Proses Manufaktur* **2023**, *7*, 63–72. https://doi.org/10.18196/jmpm.v7i1.16866.
52. Promarin, K.; Somwang, P. Thermal behavior of FDM 3D printing by using Arduino Mega 2560 approach. In *Proceedings of the 16th International Conference on Electrical Engineering/Electronics, Computer, Telecommunications and Information Technology*; IEEE: New York, NY, USA, 2019; pp. 767–770.
53. Deshpande, S.P.; Kulkarni, S.; Shah, S.; Irwin, J. Developing an open source, inexpensive, large-scale polar configuration 3D printer. *Int. J. Eng. Res. Innov.* **2019**, *11*, 13–22.
54. Alam, M.; Kader, G.; Molla, H.-O.-R.; Rokonuzzaman, A.S.M. Design, Construction and Performance Test of a Fused Deposition Modeling FDM 3D Printe. In Proceedings of the International Conference on Mechanical Engineering and Renewable Energy, Yogyakarta, Indonesia, 28–29 August 2019. Available online: https://www.researchgate.net/publication/349324030 (accessed on 25 August 2025).
55. Kamal, M.; Essam, K.; Gamal, M.; Ali, Z.; Samir, A.; Ahmed, E.; Mohamed, A.; Hesham, R.; Zayed, N.; Fouda, K. 3D Construction Printer. In Proceedings of the 5th International Undergraduate Research Conference, Cairo, Egypt, 9–12 August 2021; pp. 450–452.
56. Timperley, S.; Stec, G.; Miller, D. Timperley 1 Preliminary Design of a 3D Printing System for Creating Infinitely Large Structures in Space. In Proceedings of the 38th Annual Small Satellite Conference, Logan, UT, USA, 3–8 August 2024; pp. 1–9.
57. Sharma, S.; Harish; Nikam, S.B. XY-Drawing Robot using Arduino. *Int. J. Innov. Res. Technol.* **2019**, *6*, 170–173.
58. Shigley, J.E.; Mischke, C.R.; Budynas, R.G. *Mechanical Engineering Design*, 7th ed.; McGraw-Hill: New York, NY, USA, 2004.
59. Popescu, D.; Florea, A.; Popescu, R.; Roibu, H. 3D Printing for the Development of Robots by the Students. In Proceedings of the *27th EAEEIE Annual Conference*; IEEE: New York, NY, USA, 2017; pp. 1–6.
60. Ismaranatasia, W.; Setiawan, B.; Subiyantoro, S. Kendali Motor Stepper untuk Pergerakan Sumbu X, Y, Z pada 3D Printer Simetris Bilateral. *J. Elkolind* **2021**, *8*, 66–75. Available online: https://www.researchgate.net/publication/308568286_Vulnerability_analysis_of_desktop_3D_printer_software (accessed on 25 August 2025).
61. Hadef, M.W. *Conception et Realisation d'une Imprimante 3D*; Université Mohamed Khider de Biskra: Biskra, Algeria, 2019.
62. Devijver, S. Building Your Own 3D Printer an Introduction. Available online: https://www.scribd.com/document/534946917/Building-Your-Own-3D-Printer (accessed on 25 August 2025).
63. Honiball, J.R.; Pepper, M.S.; Prinsloo, E. Step-by-step assembly and testing of a low-cost bioprinting solution for research and educational purposes. *MethodsX* **2021**, *8*, 101186. https://doi.org/10.1016/j.mex.2020.101186.
64. Butt, J.; Bhaskar, R.; Mohaghegh, V. Analysing the effects of layer heights and line widths on FFF-printed thermoplastics. *Int. J. Adv. Manuf. Technol.* **2022**, *121*, 7383–7411. https://doi.org/10.1007/s00170-022-09810-z.
65. Evans, B. Calibrating your printer. In *Practical 3D Printers: The Science and Art of 3D Printing*; Springer: Berlin/Heidelberg, Germany, 2012; pp. 49–74.
66. Li, L.; McGuan, R.; Isaac, R.; Kavehpour, P.; Candler, R. Improving precision of material extrusion 3D printing by in-situ monitoring & predicting 3D geometric deviation using conditional adversarial networks. *Addit. Manuf.* **2021**, *38*, 101695. https://doi.org/10.1016/j.addma.2020.101695.
67. Jaksa, L.; Pahr, D.; Kronreif, G. Lorenz. Calibration Dependencies and Accuracy Assessment of a Silicone Rubber 3D Printer. *Inventions* **2022**, *7*, 35. https://doi.org/10.3390/inventions7020035.